THE GEOLOGICAL SOCIETY OF AMERICA®

Timing and amount of southern Cascadia earthquake subsidence over the past 1700 years at northern Humboldt Bay, California, USA

Jason S. Padgett[1,2,†], Simon E. Engelhart[1], Harvey M. Kelsey[3], Robert C. Witter[4], Niamh Cahill[5], and Eileen Hemphill-Haley[3]

[1]*Department of Geography, Durham University, Durham DH1 3LE, UK*
[2]*Department of Geosciences, University of Rhode Island, Kingston, Rhode Island 02881, USA*
[3]*Department of Geology, Humboldt State University, Arcata, California 95524, USA*
[4]*U.S. Geological Survey, Alaska Science Center, Anchorage, Alaska 99508, USA*
[5]*Department of Mathematics and Statistics, Maynooth University, Kildare, Ireland*

ABSTRACT

Stratigraphic, lithologic, foraminiferal, and radiocarbon analyses indicate that at least four abrupt mud-over-peat contacts are recorded across three sites (Jacoby Creek, McDaniel Creek, and Mad River Slough) in northern Humboldt Bay, California, USA (~44.8°N, −124.2°W). The stratigraphy records subsidence during past megathrust earthquakes at the southern Cascadia subduction zone ~40 km north of the Mendocino Triple Junction. Maximum and minimum radiocarbon ages on plant macrofossils from above and below laterally extensive (>6 km) contacts suggest regional synchroneity of subsidence. The shallowest contact has radiocarbon ages that are consistent with the most recent great earthquake at Cascadia, which occurred at 250 cal yr B.P. (1700 CE). Using Bchron and OxCal software, we model ages for the three older contacts of ca. 875 cal yr B.P., ca. 1120 cal yr B.P., and ca. 1620 cal yr B.P.

For each of the four earthquakes, we analyze foraminifera across representative mud-over-peat contacts selected from McDaniel Creek. Changes in fossil foraminiferal assemblages across all four contacts reveal sudden relative sea-level (RSL) rise (land subsidence) with submergence lasting from decades to centuries. To estimate subsidence during each earthquake, we reconstructed RSL rise across the contacts using the fossil foraminiferal assemblages in a Bayesian transfer function. The coseismic subsidence estimates are 0.85 ± 0.46 m for the 1700 CE earthquake, 0.42 ± 0.37 m for the ca. 875 cal yr B.P. earthquake, 0.79 ± 0.47 m for the ca. 1120 cal yr B.P. earthquake, and ≥0.93 m for the ca. 1620 cal yr B.P. earthquake. The subsidence estimate for the ca. 1620 cal yr B.P. earthquake is a minimum because the pre-subsidence paleoenvironment likely was above the upper limit of foraminiferal habitation. The subsidence estimate for the ca. 875 cal yr B.P. earthquake is less than (<50%) the subsidence estimates for other contacts and suggests that subsidence magnitude varied over the past four earthquake cycles in southern Cascadia.

INTRODUCTION

Many of Cascadia's coastal wetlands host extensive stratigraphic evidence of coseismic subsidence induced by earthquake rupture on the subduction megathrust. Over three decades of coastal paleogeodetic research on these natural archives has greatly improved our understanding of Cascadia plate boundary processes (Atwater, 1987; Darienzo, 1987; Peterson and Darienzo, 1991; Atwater, 1992; Nelson, 1992; Nelson et al., 1996a; Shennan et al., 1996; Atwater and Hemphill-Haley, 1997; Kelsey et al., 2002; Witter et al., 2003; Hawkes et al., 2010, 2011; Engelhart et al., 2013a; Wang et al., 2013; Milker et al., 2016). However, current coastal data sets do not resolve fundamental questions in Cascadia subduction zone science, such as the estimation and variability of past earthquake magnitude and the potential for persistent earthquake rupture boundaries. These questions require, in part, better earthquake chronologies and thus prompt the first question. Given adequate radiocarbon age determinations for contacts that represent subduction zone earthquakes, which Bayesian age models optimally model earthquake ages? Additionally, one of the challenges of better defining the variability in rupture length and magnitude of past subduction zone earthquakes bears on the uncertainty of evidence used to correlate paleoearthquake histories from one paleoseismic site to others along the margin. Thus, the other outstanding question we address is, what is the level of resolution needed, both for age ranges for specific paleoearthquakes and subsidence amounts for specific paleoearthquakes, to correlate earthquake records within study areas at one paleoseismic site or correlate earthquake records among different coastal paleoseismic sites?

Stratigraphic correlation of wetland stratigraphy within a marsh, over tens to hundreds of meters, can often be straightforward. However, correlation becomes increasingly difficult with distance, both across multiple marshes within a single estuary and over tens to hundreds of kilometers between estuaries (Nelson et al., 1996a; Milker et al., 2016). For evidence of earthquakes prior to the well-documented 1700 CE earthquake, radiocarbon dating techniques can test models of stratigraphic correlation within and across sites. Yet in many cases, radiocarbon age errors can be on the order of several hundred years, which presents difficulties when attempting to correlate stratigraphic contacts among estuaries recording earthquakes that have 200–500 year recurrence intervals, (Atwater, 1987; Adams, 1990; Nelson, 1992; Nelson et al., 1996a; Shennan et al., 1996; Atwater and Hemphill-Haley, 1997; Kelsey et al., 2002; Atwater et al., 2003; Witter et al., 2003; Nelson et al., 2008; Goldfinger et al., 2012; Enkin et al., 2013; Milker et al., 2016). Promisingly, new methods that incorporate multiple minimum and maximum limiting ages of in situ plant macrofossils found above and below subsidence contacts (Nelson et al., 2006, 2008; Kemp et al., 2013; Milker et al., 2016) and Bayesian statistics (e.g., Bronk Ramsey, 2008; Parnell et al., 2008) produce more accurate chronologies with better precision of stratigraphic ages to aid in correlation

†jason_padgett@uri.edu.

GSA Bulletin; September/October 2021; v. 133; no. 9/10; p. 2137–2156; https://doi.org/10.1130/B35701.1; 6 figures; 5 tables; 1 supplemental file.
published online 12 February 2021

(Kelsey et al., 2005; Goldfinger et al., 2012; Enkin et al., 2013; Garrett et al., 2015; Milker et al., 2016; Dura et al., 2017; Witter et al., 2019; Nelson et al., 2020).

Equally as important as defining the timing of past plate boundary rupture is quantifying the amount of coseismic vertical deformation. Early Cascadia coastal research utilized qualitative and quantitative methods to estimate coseismic subsidence with accompanying errors that were either poorly defined for qualitative approaches or typically ± 0.5–1.0 m for early quantitative methods (e.g., TWINSPAN, DCA; Shennan et al., 1996). Such errors are generally too large to distinguish differences between earthquakes or between sites. To improve estimates of coseismic subsidence, subsequent research at Cascadia has focused on the development of quantitative microfossil-based transfer functions primarily using foraminifera (e.g., Jennings and Nelson, 1992; Guilbault et al., 1995, 1996; Nelson et al., 2008; Hawkes et al., 2010, 2011; Engelhart et al., 2013a, 2013b, 2015; Milker et al., 2015, 2016). Foraminiferal-based transfer functions use the modern species-elevation relationships to relate fossil assemblages to past tidal elevations and enable researchers to assess differences in coseismic subsidence estimates. Cascadia foraminiferal transfer function analysis has been applied to one earthquake at many sites (Hawkes et al., 2011; Wang et al., 2013; Kemp et al., 2018) and over multiple earthquake cycles at a single site (e.g., Milker et al., 2016; Nelson et al., 2020). For example, Wang et al. (2013) use foraminiferal transfer function subsidence estimates to model along-strike slip heterogeneity during the 1700 CE earthquake and highlight large spatial gaps within the paleogeodetic database, e.g., northern California and Washington. Recent refinement and expansion of the Cascadia foraminiferal-based transfer function has led to development of a Bayesian transfer function (BTF), which can model non-unimodal taxa-elevation relationships, improves the availability of modern analogues for fossil samples, and is capable of handling sediment and microfossil mixing by assigning simple, informative priors based on lithology (Kemp et al., 2018).

Northern Humboldt Bay was one of the first locations recognized to contain stratigraphic evidence of past Cascadia subduction zone earthquakes (Vick, 1988; Clarke and Carver, 1992; Valentine 1992). However, the complicated stratigraphic record has led to disparate interpretations that have yet to be clarified by various research groups. For example, no consensus remains on the number of past Cascadia subduction zone earthquake-induced subsidence contacts or the magnitude of coseismic deformation archived within the wetland stratigraphy. These open questions have resulted in paleoseismic interpretations that range from three to six earthquakes over the past ~1900 years, (e.g., Vick, 1988, Clarke and Carver, 1992; Valentine, 1992; Pritchard, 2004; Valentine et al., 2012). Both limited radiocarbon constraints and a general lack of microfossil analysis likely contribute to inconsistent stratigraphic correlations and a lack of criteria for distinguishing contacts caused by megathrust earthquakes or other mechanisms. However, the development of improved chronostratigraphic methods and quantitative foraminiferal-based transfer functions makes it possible to refine the northern Humboldt Bay paleoseismic history.

The goals of this paper are to (1) provide high-quality age determinations for times of wetland subsidence within the northern Humboldt Bay estuary; (2) construct a paleoseismic chronology for the site; (3) provide high-precision estimates of subsidence during past subduction zone earthquakes; and (4) reevaluate and update regional (43.5°–40.5°N) correlations of paleoearthquakes in the southern Cascadia subduction zone. Our results suggest that northern Humboldt Bay has recorded four Cascadia subduction zone earthquakes over the past 1700 years and that the amount of coseismic subsidence and possibly earthquake magnitude varied in the four Cascadia earthquakes.

SETTING

The southern Cascadia subduction zone, from the Coos Bay coastal area to Cape Mendocino (Fig. 1), is a portion of the subduction zone where improved paleoseismic data would enable better-informed models of along-strike heterogeneity during the most recent (1700 CE) and older subduction zone earthquakes (Wang et al., 2013; Milker et al., 2016; Kemp et al., 2018). Southern Cascadia archives the temporally longest onshore paleoseismic records observed along the whole subduction zone with earthquake histories extending back 6700 years documented at the Sixes River, Bradley Lake, and Coquille River sites (Kelsey et al., 2002, 2005; Witter et al., 2003; Fig. 1). However, the two largest spatial data gaps with no paleoseismic information along the entire subduction zone are also in southern Cascadia (Fig. 1). These spatial data gaps are the ~75-km-long coastal reach north of Humboldt Bay and the ~85-km-long coastal reach north of the Crescent City area (Fig. 1B). These spatial data gaps occur because the coastal environments appear to lack a stratigraphic record that preserves relative sea-level (RSL) changes (Hemphill-Haley et al., 2019). Even though investigations at Lagoon Creek (<20 km south of Crescent City) have reported evidence for tsunami inundation as much as 3500 years ago (Abramson, 1998; Garrison-Laney, 1998), many of the freshwater lacustrine and wetland environments near Crescent City record a limited extent of stratigraphic evidence for coseismic subsidence, e.g., Sand Mine Marsh (Peterson et al., 2011; Simms et al., 2017; Hemphill-Haley et al., 2019). Finding subsidence stratigraphy in the spatial gaps north and south of Crescent City may not be realized, even with more field reconnaissance, if conditions preclude the accommodation space required to document stratigraphic evidence of late Holocene RSL changes (Kelsey et al., 2015; Dura et al., 2016). We chose an alternative approach to ultimately improve models of along-strike heterogeneity in southern Cascadia; namely, we reevaluate the paleoseismic record in northern Humboldt Bay, a site where subsidence stratigraphy has been documented but where previous legacy studies did not attain scientific consensus on the subduction zone earthquake record.

Despite northern Humboldt Bay being a focal point of southern Cascadia paleoseismic research over the past 30 years, the stratigraphic framework and paleoseismic history has remained unresolved. Vick (1988) was the first to describe the tidal wetland stratigraphy at northern Humboldt Bay and focused on the stratigraphy at Mad River Slough. Even though Vick (1988) observed five submergence contacts, based on stratigraphic mapping and six radiocarbon ages, he concluded that at least four submergence contacts represent coseismic subsidence. Subsequent investigations extended stratigraphic mapping and paleoseismic correlations beyond Mad River Slough and consequently developed both similar (Clarke and Carver, 1992; Valentine, 1992) and divergent (Pritchard, 2004; Valentine et al., 2012) interpretations. Clarke and Carver (1992), Valentine (1992), and Valentine et al. (2012) correlate stratigraphic contacts and ages to other paleoseismic data from proximate trenching and wetland sites and conclude that four to six megathrust events have occurred over the past 2000 years. In contrast, Pritchard (2004) focused solely on the tidal wetland stratigraphic record within the northern Humboldt Bay estuary and concluded that the tidal wetland stratigraphy records evidence for three to four megathrust earthquakes over the past 1900 years. Even though specific correlations and conclusions differ, the common theme throughout the research conducted at northern Humboldt Bay is that the complicated stratigraphy has restricted conclusionary findings and further research is required to refine the understanding of the paleoseismic history.

We studied stratigraphy beneath three tidal marshes that fringe the northern portion of Humboldt Bay: Mad River Slough, McDaniel Creek, and Jacoby Creek. These areas are protected and managed by the U.S. Fish and Wildlife Service

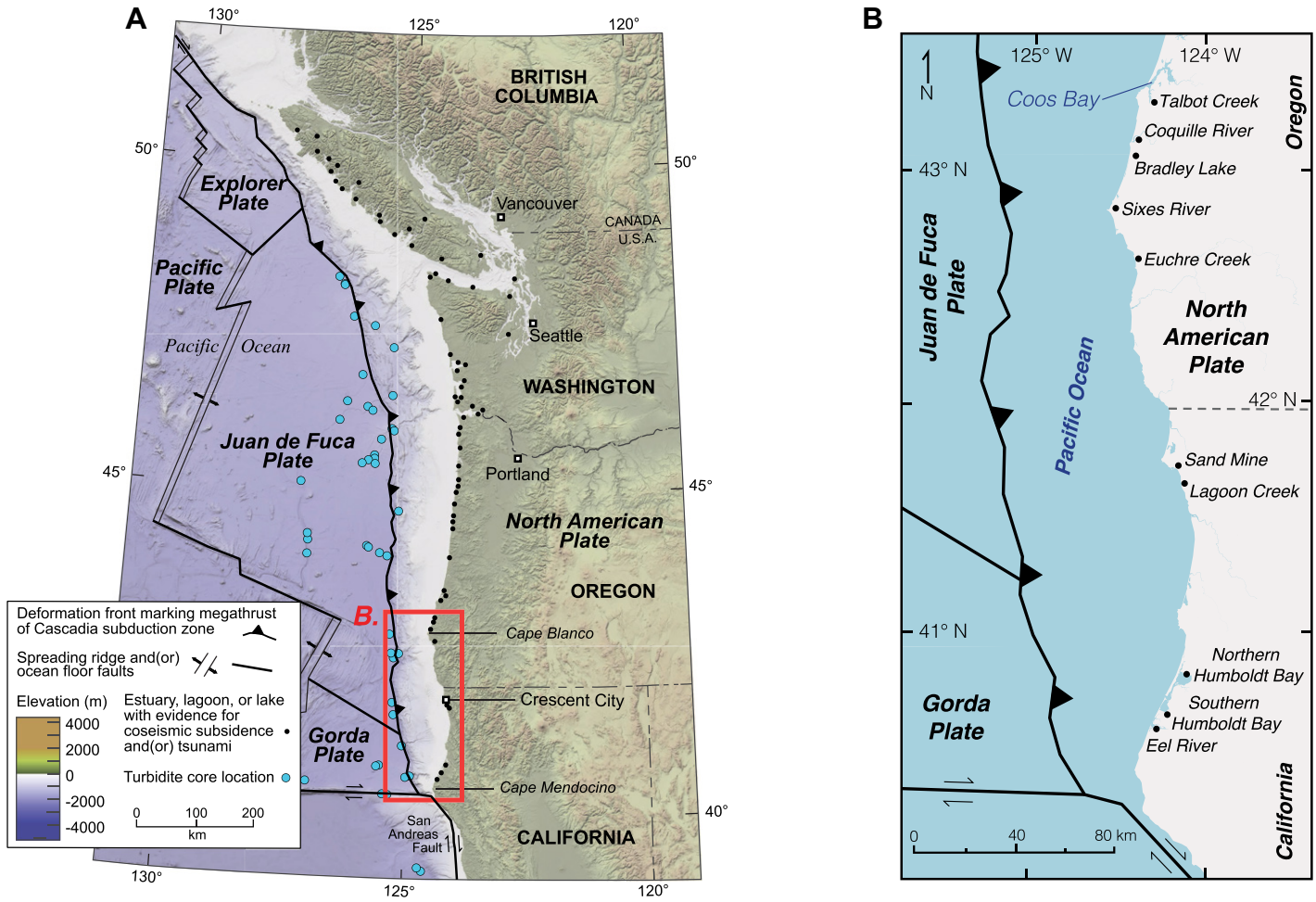

Figure 1. (A) Physiography and major features of the Cascadia subduction zone are shown. Base map data source: GEBCO Compilation Group (2019) GEBCO 2019 Grid, https://10.5285/836f016a-33be-6ddc-e053-6c86abc0788e) and modified from Nelson et al. (2020). The deformation front of the subduction zone megathrust fault on the ocean floor (black barbed line) is near the bathymetric boundary between the continental slope and abyssal plain. Dots mark estuaries, lagoons, or lakes with evidence for coastal subsidence, tsunamis, and/or turbidites accompanying subduction zone earthquakes. (B) Location map of the southern Cascadia coastline. Dots mark estuaries or lakes with evidence for coastal subsidence and/or tsunami.

Humboldt Bay National Wildlife Refuge or the city of Arcata, California (Fig. 2). Northern Humboldt Bay is separated from the Pacific Ocean by the ~20–25-m-high Lanphere-Ma-le'l Dunes (Fig. 2C; Vick, 1988; Pickart and Hesp, 2019). At the mouth of Mad River Slough, a National Oceanic and Atmospheric Administration (NOAA) tide gauge station registers the semidiurnal tidal range (mean higher high water [MHHW]–mean lower low water [MLLW]) at 2.36 m (Fig. 2C; NOAA ID: 9418865). Because over half of northern Humboldt Bay surface area is exposed at low tide, most of the environments of the lagoon system are tidal channels and low-tide mud flats (Eicher, 1987; Schlosser and Eicher, 2012). Low marshes form at elevations around mean high water (MHW), and high marshes form at elevations around MHHW (Pritchard, 2004).

Flora and fauna within northern Humboldt Bay are typical for Cascadia tidal wetland plant and animal distributions (Pritchard, 2004; Hawkes et al., 2010, 2011; Engelhart et al., 2013b, 2015; Kemp et al., 2018). Plant communities of lower marsh environments, around mean tide level (MTL), include *Distichlis spicata*, *Salicornia virginica*, *Spartina densiflora*, and *Triglochin maritimum* (Eicher, 1987). In high marsh environments, plant communities include *Castilleja exserta*, *Distichlis spicata*, *Grindelia* spp., *Jaumea carnosa, Spartina alterniflora*, and *Triglochin maritimum* (Eicher, 1987). Kemp et al. (2018) show that intertidal benthic foraminiferal communities are comparable along the west coast of North America from ~35.5°–50°N. Benthic foraminiferal communities differ along an intertidal gradient such that higher marsh environments, around MHHW, are often dominated by *Trochaminita* spp., *Haplophragmoides* spp., *Balticammina pseudomacrescens*, *Trochammina inflata*, and *Jadammina macrescens*. Whereas at elevations from ~MHW down to MTL, increasing percentages of *Miliammina fusca*, *Ammobaculites* spp., *Reophax* spp., and calcareous foraminifera species are reported (Guilbault et al., 1995, 1996; Nelson et al., 2008; Hawkes et al., 2010, 2011; Engelhart et al., 2013a, 2013b; Pilarczyk et al., 2014; Milker et al., 2015, 2016; Kemp et al., 2018).

We selected three study sites because the existing wetland stratigraphic framework reflects a complicated stratigraphic record of earthquake subsidence. The stratigraphic sections typically consist of repeated abrupt mud-over-peat and mud-over-upland soil contacts, where a peat or

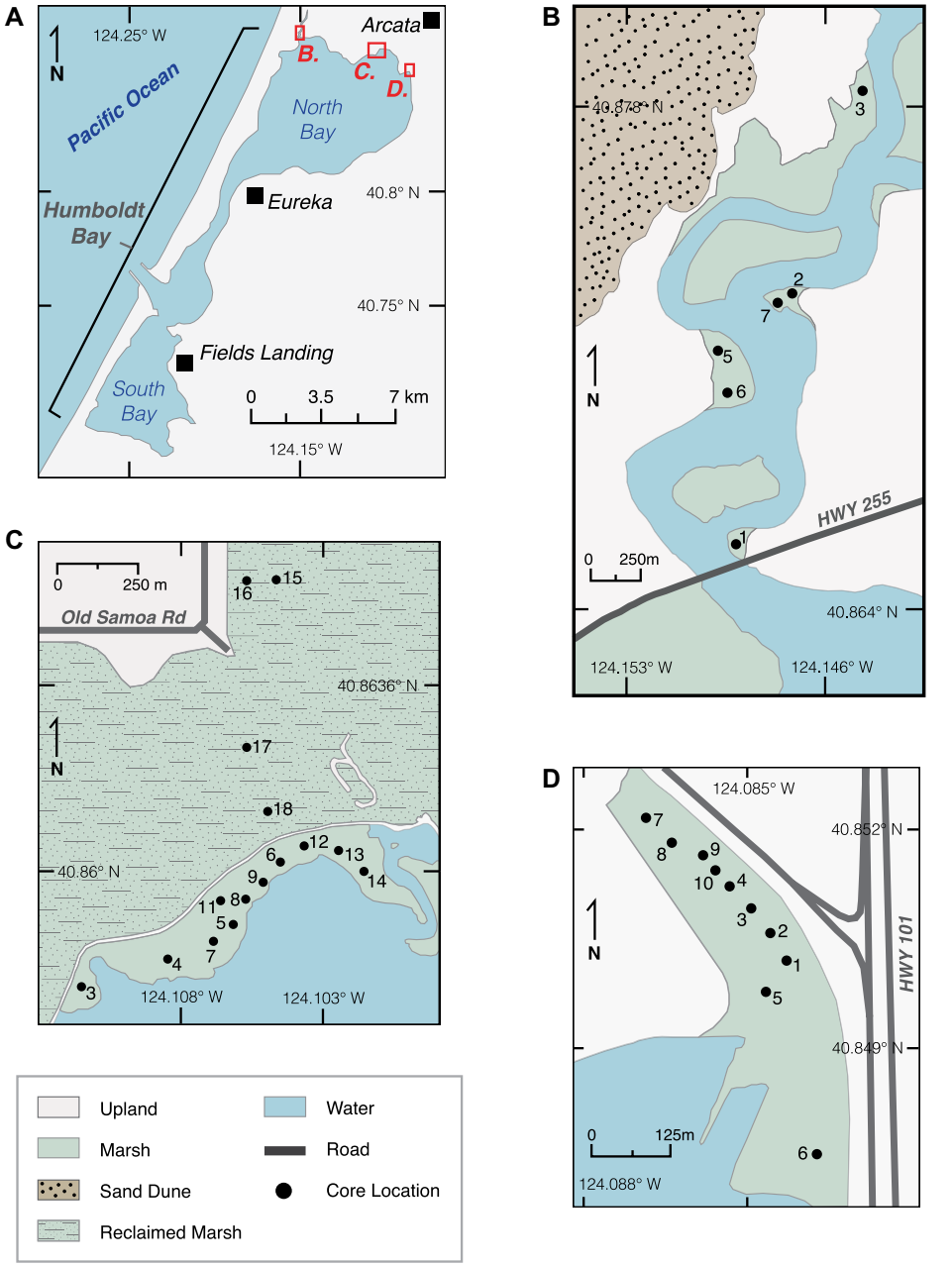

Figure 2. Location maps show (A) Humboldt Bay, (B) Mad River Slough, (C) McDaniel Creek, and (D) Jacoby Creek.

upland soil is sharply overlain by tidal mud and then the tidal mud gradually grades upward into an overlying, organic-rich unit.

RESEARCH APPROACH AND METHODS

To evaluate if stratigraphy is evidence of megathrust-induced, land-level changes, we utilize a strategy refined by over three decades of research along the Cascadia margin through the context of land-level changes expressed by contrasting stratigraphic units within intertidal sediments (Atwater, 1987; Hemphill-Haley, 1995; Nelson et al., 1996a; Witter et al., 2001; Kelsey et al., 2002; Witter et al., 2003; Hawkes et al., 2011; Engelhart et al., 2013a; Milker et al., 2016; Shennan et al., 2016). Our approach utilizes four of the criteria proposed by Nelson et al. (1996a) and Shennan et al. (2016) to test for identifying coseismic subsidence in tidal-wetland stratigraphic sequences. These criteria are (1) lateral extent of stratigraphic contacts; (2) suddenness of submergence; (3) amount of submergence; and (4) regional synchroneity of submergence, which is determined by employing stratigraphic mapping, lithostratigraphic analysis, foraminiferal analysis, and radiocarbon dating techniques combined with potential correlations with other plate boundary earthquake records in southern Cascadia. We do not discuss the "coincidence of tsunami deposit" criterion because we found no evidence for a tsunami deposit above any buried, organic-rich unit. The ~20–25-m-high, Lanphere-Ma-le'l Dunes may have protected northern Humboldt Bay from tsunami inundation (Vick, 1988; Pickart and Hesp, 2019).

Our research approach is threefold: (1) lithostratigraphic analysis (describe subsurface stratigraphy at multiple core locations across three sites), (2) chronologic analysis using Bayesian age models (constrained by radiocarbon accelerator mass spectrometry [AMS] ages of plant macrofossils), and (3) relative sea-level reconstructions (estimate paleoenvironmental elevation changes using fossil foraminiferal data and an existing BTF; Kemp et al., 2018).

Lithostratigraphic Analysis

Stratigraphic Description and Sampling

We compiled stratigraphic descriptions from 31 core locations over a >6 km transect at Mad River Slough (6), McDaniel Creek (15), and Jacoby Creek (10) moving west to east (landward) along the northern shore of northern Humboldt Bay (Fig. 2). Wetland stratigraphy consists of clastic mud and interbedded organic-rich units. A clastic "mud" refers to a gray to olive gray massive to finely (1–3 mm) bedded silt and clay. An "organic-rich unit" refers to a dark oxidized salt marsh peat or an upland soil. A "submergence contact" is either a mud-over-peat or mud-over-upland soil contact.

Using a 30-mm-wide gouge core, we mapped abrupt (1 mm), sharp (1–5 mm), clear (5–10 mm), and gradual (>10 mm) submergence contacts up to ~4 m depth below the ground surface. Grain size, sedimentary structures, contacts, thickness, and facies changes were described in the field using general stratigraphic methods in combination with the Troels-Smith (1955) method for describing organic-rich sediment. Stratigraphic unit descriptions include peat, muddy peat, peaty mud, and mud. Organic percentages determined by qualitative field assessment (Troels-Smith, 1955) for peat, muddy peat, and peaty mud are 100%–75%, 75%–50%, and 50%–25%, respectively. Silt and clay units that consist of <25% organics by volume are described as "mud." For lab analyses, we selected representative segments (50 cm) of key

stratigraphic intervals that visually contained the sharpest contacts between the mud-over-peat and mud-over-upland soil contacts and/or abundant in situ plant macrofossils. Samples were collected for radiometric and biostratigraphic analyses using either an Eijkelkamp peat sampler or a 60-mm-gouge core.

Stratigraphic Imaging

Contact sharpness and continuity is not always clear from optical inspection. Therefore, we followed recent studies in Cascadia (e.g., Goldfinger et al., 2012; Milker et al., 2016) and Alaska (e.g., Briggs et al., 2014; Witter et al., 2019) and obtained high-resolution imagery to analyze fossil core density contrasts. We examined density imagery of multiple representative cores prior to selecting the optimal core and stratigraphic intervals for counting foraminifera as well as selecting material for radiocarbon dating. Computerized tomography (CT) scans were conducted at Oregon State University College of Veterinary Medicine and Rhode Island South County Hospital following the methods outlined in Rothwell and Rack (2006) and Davies et al. (2011). At Oregon State University, density measurements were collected at 120 kVp and 200 mA and a pitch of 0.5s (100 mAs) using a Toshiba Aquilion 64-slice computed tomography system. For visualization purposes, the resulting images were processed with a "bone" algorithm to generate coronal images every millimeter across the core. At Rhode Island South County Hospital, density scans were collected with 32-slice GE LightSpeed scanner at 120 kVp and 200–600 mA (depending on the fossil core thickness) core and a pitch of 0.969:1. X-radiation (X-ray) images, collected with a Shimadzu UD150B-40 and imaged with a Fuji FCR XL-2 at the University of Rhode Island Health Center, also illuminate density differences within the collected sediment cores. The fossil core images were processed using Horos and Adobe Illustrator software.

Surveying to Sea-Level Datum

Sample elevations for each core were acquired using real-time kinematic-global positioning system (RTK-GPS). Data collected by the RTK-GPS was post-processed using Online Positioning User Service, https://www.ngs.noaa.gov/OPUS/, to obtain North American Vertical Datum 1988 (NAVD88) orthometric elevations. To establish elevations with respect to a tidal datum, we took RTK-GPS measurements of the tidal benchmarks associated with the temporary tide gauge installation (12/01/1978–03/31/1979) at Mad River Slough (NOAA ID: 9418865). The vertical precision of the RTK measurements is less than 4 cm.

Chronologic Analysis

Radiocarbon Dating

Plant macrofossils were collected from above and below key contacts to provide 24 bracketing maximum and/or minimum ages for each organic-rich unit upper contact at all three sites. We focused on samples that were found in growth position and/or close (<3 cm) to submergence contacts and that have the potential to tightly constrain the timing of the organic-rich unit burial, such as rhizomes of salt-marsh plants that have a known relationship to the surface of the marsh (n = 13). We also collected detrital fragments of plants including stems (n = 8) and wood fragments (n = 1) and seeds and seed casings (n = 2). Discrete stratigraphic intervals that range from 0.5 cm to 1.5 cm were sampled from cores and disaggregated on a glass plate under a binocular microscope. Occasionally, high-resolution CT scans and X-radiographic images aided in targeting organic materials to be extracted from sediments. Selected material, usually plant rhizome, stem, or seed, was cleaned of all attached sediment particles and rootlets and then oven dried at ~50 °C for 24 h (Kemp et al., 2013; Nelson, 2015; Törnqvist et al., 2015). Once dried and weighed, samples were sent to the National Ocean Science Accelerator Mass Spectrometer (NOSAMS) Laboratory at Woods Hole Oceanographic Institute for analysis. The AMS radiocarbon age results were calibrated with OxCal (version 4.2.4; Bronk Ramsey and Lee, 2013) using the IntCal13 calibration curve for terrestrial samples (Reimer et al., 2013) and are reported with the standard two-sigma uncertainty in calendar years before 1950 (cal yr B.P.).

Bayesian Age Models

We developed a representative, estuary-wide composite stratigraphy to be used in the construction of three Bayesian age models. The composite stratigraphy incorporates maximum and minimum plant macrofossil samples that were selected as close to the upper contacts of the buried, organic-rich units as possible. Outlier ages, as well as anomalously older and younger ages than stratigraphic position would suggest, were not incorporated into the composite stratigraphic section used in model development.

Bayesian age-depth modeling has been used by many RSL investigations that seek to refine the timing of past changes in RSL and decrease the error envelopes of sediment accumulation histories (e.g., Garrett et al., 2015; Dura et al., 2017; Witter et al., 2019). Model choice is a vital component of reducing timing uncertainties, and the consistency of accumulation rates should be considered (Wright et al., 2017). If deposition is seasonal, steady, and predictable, for example a lake bottom, then an OxCal U-sequence command (Bronk Ramsey, 2008, 2009) would be a good age model option because deposition is assumed to be fairly uniform. However, if a sedimentation rate is variable, then models that can account for randomness in deposition can be more suitable, e.g., Bchron (Parnell et al., 2008) or OxCal P-sequence (Bronk Ramsey, 2008, 2009). In contrast, if only an order is known, a more conservative model such as OxCal Sequence command is appropriate, which only defines an order for events and groups of events (Bronk Ramsey, 1995). In regard to the ability to capture sedimentation rate variability, within their confidence intervals OxCal P-sequence and Bchron outperform other age modeling programs (Trachsel and Telford, 2017; Wright et al., 2017).

Typically, tidal wetland stratigraphic investigations obtain a chronologic data set, construct a numerical age-depth model, and test the results to other regional data sets. However, little work has considered the potential differences in the age estimate results that could be imposed by the numerical age model of choice. Moreover, often only the modeling program is cited without the specific type of model identified and/or explained (Milker et al., 2016; Nelson et al., 2020). We attempt to address this gap by comparing useful Bayesian age-depth models to assess the variability in age estimates that may be imposed by model choice.

Three Bayesian age models with different assumptions are utilized to estimate time of organic-rich unit burial, OxCal Sequence, and P-sequence commands (Bronk Ramsey, 1995, 2008, 2009), and Bchron (version 4.3.0; Haslett and Parnell, 2008). The OxCal Sequence command only incorporates the relative positioning of the age constraints within the composite stratigraphy, i.e., it does not incorporate a modeled sedimentation rate to further refine the ages of subsidence contacts. In contrast, OxCal P-sequence and Bchron model sedimentation rates are based on age constraint depths and accumulation rate parameters (Trachsel and Telford, 2017). OxCal P-sequence allows for variable sediment accumulation as a Poisson process controlled by the user defined *k-parameter*. We follow the approach of Bronk Ramsey (2008) and Enkin et al. (2013) for determining the optimal value of *k* by selecting the highest *k* value that agrees with the actual dating information. Bchron also incorporates sample depths to further constrain the age estimate by modeling a sedimentation rate between age constraint intervals but, in contrast to OxCal P-sequence,

does so without the user defining a sedimentation rate parameter. Instead, Bchron is based on modeling piecewise linear accumulations, where increments are independent and arrive in a Poisson fashion, which allows for abrupt changes in accumulation rates (Haslett and Parnell, 2008; Trachsel and Telford, 2017). Modeled sedimentation rates trim the predicted age and result in a more precise estimate. However, the accuracy depends on an appropriate density of radiocarbon dates that can identify changes in sedimentation rate that may be expected post-earthquake and that exceed the long-term (centennial-scale) average. Using more than one Bayesian age modeling technique, each with different assumptions, enables us to assess the impacts of model choice on the variability of age estimates.

Regional Paleoseismic Timing Correspondence

Based on our comparison of Bayesian modeling techniques, which is described below (see Results), we prefer results from the OxCal Sequence modeling technique. Thus, we compare the age distributions derived from OxCal Sequence results from northern Humboldt Bay with the timing of plate-boundary earthquakes at other sites along the southern Cascadia coastal estuarine and lacustrine environments from 43.5°–40.5°N, which include Eel River (Li, 1992), southern Humboldt Bay (Patton, 2004), Lagoon Creek (Abramson, 1998; Garrison-Laney 1998), Bradley Lake (Kelsey et al., 2005), Coquille River (Witter et al., 2003), and Talbot Creek, which is a tributary to South Slough in the Coos Bay region of southern Oregon (Milker et al., 2016). We also compare offshore turbidite data that have been interpreted to reflect shaking produced by great earthquakes (Goldfinger et al., 2012). We do not include paleoseismic data from Sixes River in our comparison because, since ~2000 years ago, the lower Sixes River Valley has not recorded (or minimally recorded) coseismic subsidence. i.e., earthquakes did not drop the lower valley into the intertidal range (Kelsey et al., 2002). Bradley Lake and Lagoon Creek are coastal lacustrine environments that are inferred to have recorded tsunami inundation coincident with plate-boundary earthquakes. Eel River, southern and northern Humboldt Bay, Coquille River, and Talbot Creek are estuarine marshes that have recorded evidence of both coseismic land-level changes and occasionally subsequent tsunami inundation. Offshore turbidite chronology provides the longest stratigraphic records of Cascadia subduction zone paleoseismic history. Each location included in our comparison has recorded evidence of megathrust earthquakes within the past ~2000 years.

Relative Sea-Level Reconstructions

Foraminifera

Fossil foraminifera species assemblages are indicative of paleo-intertidal environments. We followed standard sample preparation and analysis techniques for fossil foraminifera found within wetland stratigraphy (e.g., Scott and Medioli, 1982; de Rijk, 1995; Horton and Edwards, 2006). Fossil foraminifera were concentrated by sieving 1 cm intervals of sediment (~3 cm^3) from collected cores over 500- and 63-micron sieves and retaining the material between those size fractions. The 500-micron sieve was checked for larger foraminifera before material was discarded. Fossil samples were analyzed until at least 200 dead foraminifera were identified or until the entire sample was enumerated (Fatela and Taborda, 2002). Following Kemp et al. (2018), only samples with >30 foraminifera were used in the production of quantitative RSL reconstructions because low abundances may reflect a transported assemblage and/or may not be representative of the depositional environment. Foraminifera were identified following taxonomy based on Hawkes et al. (2010) and Milker et al. (2015). Additionally, we combine *Haplophragmoides* spp. following Kemp et al. (2018). We apply a pairwise comparison test of modern and fossil foraminiferal assemblages to confirm that all fossil assemblages have modern analogs.

Transfer Function

Sudden RSL change caused by subsidence during past great earthquakes along the Cascadia coastal margin can be quantified using fossil foraminifera (found within subsidence stratigraphy) and a transfer function (Guilbault et al., 1995, 1996; Nelson et al., 2008, Hawkes et al., 2010, 2011; Engelhart et al., 2013a, 2013b; Wang et al., 2013; Milker et al., 2016; Kemp et al., 2018). Early fossil foraminifera transfer functions utilized a local (same site) training set of foraminiferal assemblages and tidal elevations (Guilbault et al., 1995, 1996; Nelson et al., 2008). Later efforts progressed to regional modern training sets, where more robust taxa-elevation relationships were constructed based on compilations from several marsh sites (Hawkes et al., 2010, 2011; Engelhart et al., 2013b; Wang et al., 2013; Milker et al., 2016). Generally, a larger modern data set provides a higher diversity of modern analogs and covers more natural variability; but a larger modern data set is often accompanied by reduced precision (Horton and Edwards, 2005). More recently, Kemp et al. (2018) developed a BTF that incorporates an extended West Coast modern foraminifera training set, allows for flexible species-response curves, and can formally incorporate information about elevation from additional proxies, e.g., other microfossil groups, $\delta^{13}C$, or lithologic/stratigraphic context, which combine to produce more informed estimates of RSL reconstruction and extends applicability of the methodology (Cahill et al., 2016; Holden et al., 2017). We follow Kemp et al. (2018) and use lithology to provide constraints for RSL reconstructions. The lithology ranges from either clastic dominated (tidal flat) to low salt-marsh sediment, which most likely accumulates at elevations between mean low water (MLW) and MHHW (20–200 sea water level index [SWLI]) or organic-rich, high salt marsh, which most likely accumulates at elevations around MHW to the highest occurrence of foraminifera (HOF; 180–252 SWLI; Kemp et al., 2018). Although clastic sediment can accumulate at elevations below 20 SWLI, we follow the assumptions of Kemp et al. (2018). The BTF does not incorporate a lithologic prior assignment of a forest or upland soil unit because such environments occur above HOF and foraminifera cannot inform such elevations. To evaluate if a fossil assemblage has a modern analog, we used the Bray-Curtis distance metric. Due to low species diversity, a threshold of less than the 20th percentile is appropriate for salt marsh foraminifera modern and fossil assemblage pairings (Kemp and Telford, 2015).

RESULTS

We first describe wetland stratigraphy across the three sites. Then we present radiocarbon ages that constrain the timing of organic-rich unit burial. Using the radiocarbon age results, we correlate buried, organic-rich units among all the sites using lithology, depth, and age. Next, we present radiocarbon age modeling to assign age ranges to the submergence contacts. Finally, using foraminiferal analyses, we present estimates of subsidence across submergence contacts at McDaniel Creek.

We focus our foraminiferal analysis on stratigraphic sections collected at McDaniel Creek because it archives the largest spatial extent of subsidence stratigraphy within northern Humboldt Bay. One exception is analysis of a single stratigraphic section from Mad River Slough because of the limited spatial extent of a contact that is not found at McDaniel Creek. To derive a subsidence estimate we use the distributions of the reconstructed RSL elevations from the first unmixed centimeter intervals above and below the subsidence contact.

Wetland Stratigraphy

In cores, we observed gray mud units sharply overlying dark organic-rich units, which we refer

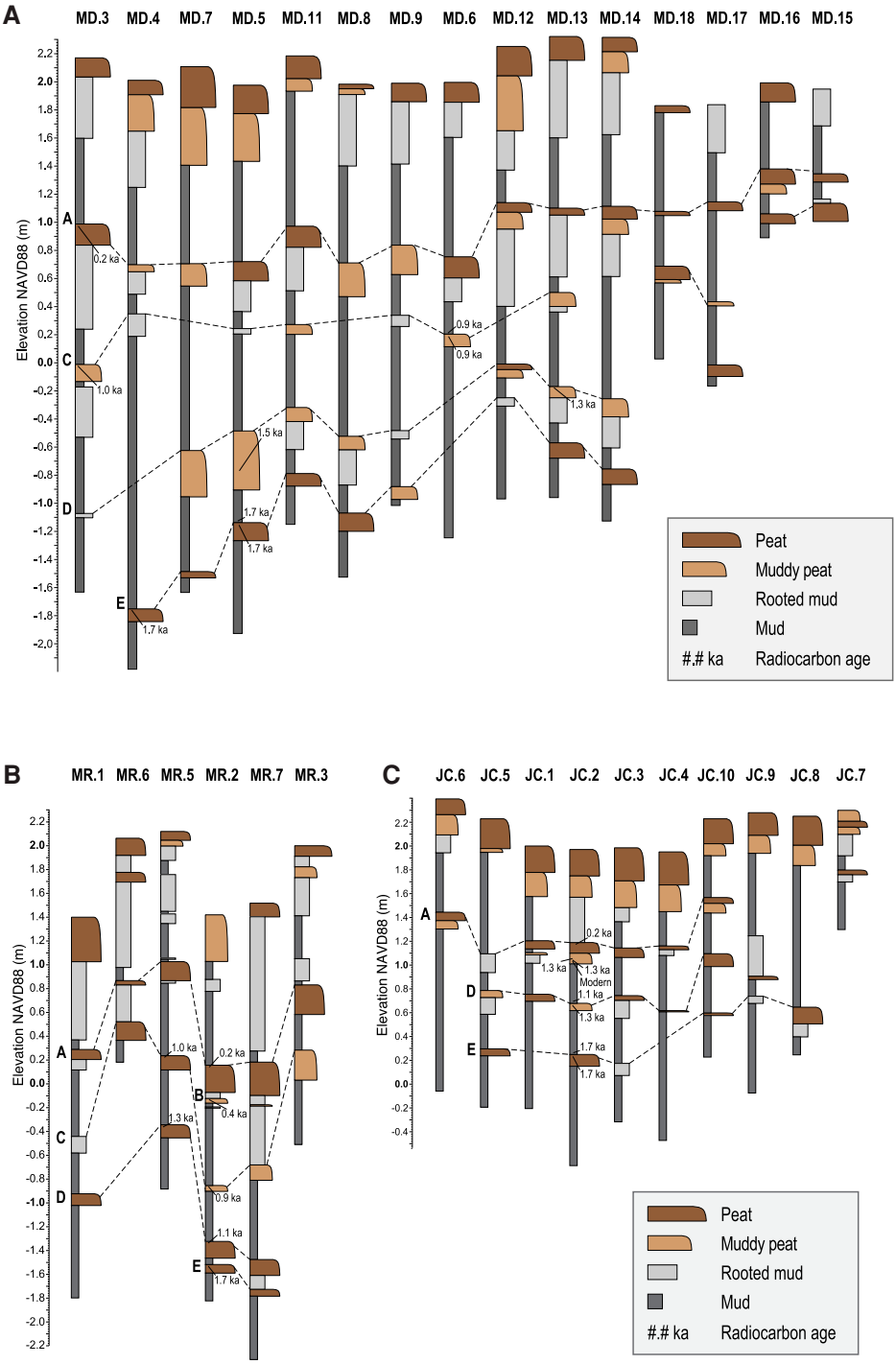

Figure 3. Simplified lithostratigraphy of northern Humboldt Bay at (A) McDaniel Creek, (B) Mad River Slough, and (C) Jacoby Creek. Core depths are shown relative to present-day elevation. Calibrated ^{14}C ages (ka; mode of ^{14}C distribution rounded to the nearest century) are shown for samples above and below contacts (more complete radiocarbon age data in Table 2). The letters A, B, C, D, and E refer to submergence contacts that are tested to be evidence for megathrust-induced subsidence. See Table 2 for more complete radiocarbon age data.

to as a submergence contact (Fig. 3; Table 1). The organic-rich units contain humified organic matter and plant macrofossils. The clastic muds contain sparse plant macrofossils and were often massive and occasionally finely bedded. We did not observe any sand layers between an organic-rich unit and overlying mud across the estuary. In general, the shallowest organic-rich units are well-defined and widespread, while deeper organic-rich units are often less distinct, more humified, and have a more restricted lateral extent. Stratigraphic mapping identified five submergence contacts at Mad River Slough, four submergence contacts at McDaniel Creek, and three submergence contacts at Jacoby Creek (Fig. 3; Table 1). We reoccupied previously described wetland stratigraphic sections (Vick, 1988; Clarke and Carver, 1992; Valentine, 1992; Pritchard, 2004; Valentine et al., 2012) and further extended the spatial extent of wetland stratigraphic mapping in northern Humboldt Bay. In doing so, we document submergence contacts that have not been previously described at McDaniel Creek and the Jacoby Creek marshes.

Mad River Slough

We reoccupied six coring sites of Vick (1988) in the southern portion of Mad River Slough and observed similar stratigraphy (Fig. 3B). We observed five submergence contacts at *MR.2* and *MR.7*, but based on lithology and depth we can correlate four submergence contacts across the six-location survey at Mad River Slough (Figs. 2B and 3B; Table 1). Core top elevations differ from the west to the east side of the main tidal channel and are 2.1 m and 1.4 m, respectively (NAVD88). The shallowest organic-rich unit is a relatively thick, well-developed peat that is observed at every core location. The second deepest from the organic-rich unit at the surface is a relatively thin peat that is observed $<$8 cm below the lower contact of the overlying peat unit. The second and fifth deepest organic-rich units were only observed at the same two core locations: *MR.2* and *MR.7* (Figs. 2B and 3B; Table 1). The third deepest organic-rich unit was observed at every core location and ranges from a rooted mud to a peat between the core locations. The fourth deepest, described as a peat unit, was observed on both sides of the main channel. The deepest organic-rich unit is a humified peat. Although all the submergence contacts are at least clear, the fourth and fifth deepest organic-rich units have less distinct upper contacts (Table 1). In summary, five submergence contacts were observed at two core locations, three submergence contacts were observed at two core locations, and two submergence contacts were observed at two core locations (Fig. 3B). Mad River Slough archives the highest amount of stratigraphic variability throughout the estuary (Fig. 3B; Table 1).

McDaniel Creek

We expanded upon the stratigraphic descriptions of Pritchard (2004) by describing 15 core

TABLE 1. ATTRIBUTES OF BURIED, ORGANIC-RICH UNITS FROM CORES

Numbered (by depth) buried, organic-rich unit upper contact	Number of cores that sample the unit	Depth range of buried, organic-rich unit upper contact (cm)	Nature of buried, organic-rich unit upper contact*	Thickness range of organic-rich unit (cm)	Thickness range of mud deposit overlying buried, organic-rich unit (cm)
Mad River Slough					
1	6	94–136	5a, 1s	15–35	68–97
2	2	169–174	1a, 1s	3–4	5–7
3	6	184–227	3a, 2s, 1c	8–20	24–65
4	4	234–275	3s, 3c	15–20	32–72
5	2	295–303	2c	4–12	12–17
McDaniel Creek					
1	15	78–145	11a, 3s, 1c	5–24	60–110
2	9	171–213	3a, 4s, 2c	4–12	18–62
3	10	226–257	2a, 4s, 4c	4–33	32–110
4	9	250–380	2s, 4c, 2g	4–13	16–196
Jacoby Creek					
1	8	48–116	6a, 2s	8–18	11–86
2	6	113–133	2s, 4c	5–11	18–70
3	6	163–203	1s, 4c, 1g	4–8	16–118

Note: Depths and thicknesses are rounded to the nearest centimeter; thicknesses <1 cm are rounded to the nearest millimeter.
*Contacts: a—abrupt, 1 mm; s—sharp, 1–5 mm; c—clear, >5–10 mm; g—gradual, >10 mm. Number refers to number of observations.

locations farther west-northwest (Figs. 2A and 3C). South of the dike, core elevations range from 2.0 m to 2.3 m, and north of the dike core elevations range from 1.8 m to 2.0 m (NAVD88).

Based on lithology and depth, we correlate four submergence contacts across a 15-core survey at the McDaniel Creek site. The shallowest organic-rich unit was observed at every core location survey and varies from a muddy peat to a peat both across multiple core locations and also within the unit. The second deepest organic-rich unit was observed at nine locations and varies from a rooted mud to a muddy peat between locations and within the unit. The third deepest organic-rich unit was observed at 10 locations and varies from rooted mud to a peat between locations and within the unit. The fourth deepest organic-rich unit was observed at nine core locations and is a humified organic-rich unit. We observed a less distinct upper contact at the fourth deepest organic-rich unit than at the shallower organic-rich units (Table 1). In summary, four submergence contacts were observed at five core locations while three submergence contacts were observed at seven core locations. The organic content of both the second and third deepest buried, organic-rich units increases to the northeast toward the modern channel. McDaniel Creek archives the largest lateral extent of submergence contacts throughout the estuary.

Jacoby Creek

Similar to previous investigations (Valentine, 1992; Pritchard, 2004), we observed one submergence contact close to the mouth of Jacoby Creek at *JC.6*. We extended stratigraphic mapping ~200–400 m farther to the north at the marsh and observed three submergence contacts within the top 200 cm of the marsh stratigraphy (Figs. 2D and 3C).

Across a 10-core transect, three submergence contacts were correlated based on depth in cores and lithology. Elevations of the core tops range from 1.95 m to 2.39 m (NAVD88). At the northern and southern extents of the survey transect in cores only one submergence contact was observed. At four core locations in the mid-section of the marsh, three submergence contacts were observed within 200 cm below the salt marsh surface. The shallowest organic-rich unit was observed at eight core locations and ranges from bold, well-developed peat to a muddy peat within the unit. The second deepest organic-rich unit was observed at seven core locations and ranges from a peat to a muddy peat both within the unit and across multiple core locations. The deepest organic-rich unit was observed at six core locations, is a highly humified upland soil, and overlies pebbly sand alluvial sediments. In summary, at Jacoby Creek, we observed three submergence contacts at four core locations, two submergence contacts at three locations, and one submergence contact at three core locations. Jacoby Creek core sites have the highest core top elevations, cover the smallest surface area, and have the shallowest wetland stratigraphic section in northern Humboldt Bay.

Radiocarbon Ages

We obtained 24 radiocarbon ages of plant macrofossils to determine the timing of paleoenvironmental changes across the upper contacts of buried, organic-rich units (Table 2). Whenever possible, we used identifiable plant material. Both minimum and maximum age samples were found above and below the three deepest submergence contacts and constrain the timing of those paleoenvironmental changes. Although we obtained 24 radiocarbon ages, we exclude three dates identified as outliers in stratigraphic sequences. We infer that downward bioturbation and/or root penetration has resulted in a younger age than stratigraphic position would suggest (sample *JC.14.02.D.100–101*), and detrital reworking and deposition has resulted in anomalous older dates than stratigraphic position suggests (*JC.14.02.D.103–104* and *JC.14.02.D.103–105*) (Fig. 3C; Table 2). The calibrated ages range from modern to 1575–1707 cal yr B.P., indicating that the sediments accumulated over the last two millennia (Table 2).

From Mad River Slough we obtained seven radiocarbon ages that provide a 1700-year chronology (Table 2). One maximum age (307–1 cal yr B.P.) from the shallowest organic-rich unit falls within last ~300 yr radiocarbon calibration plateau. The age of a *D. spicata* rhizome derived from the second deepest buried, organic-rich unit is consistent with previous paleoseismic dating results of the same unit (e.g., Valentine et al., 2012). Previous investigations have suggested that the second deepest submergence contact could represent subsidence from a Cascadia subduction zone earthquake; however, we did not observe similar stratigraphy or radiocarbon age anywhere else within the marsh or across the estuary (Fig. 3; Tables 1 and 2). Maximum ages from the third deepest organic-rich unit are consistent (956–912 cal yr B.P. and 956–802 cal yr B.P.) and aid in correlation of stratigraphy across the marsh. The burial timing of the fourth organic-rich unit is constrained by a minimum age (1057–961 cal yr B.P.) and a maximum age (1280–1183 cal yr B.P.). Within the deepest organic-rich unit, we dated roughly 25 *Atriplex* and *Potamogeton* seeds, which provide maximum age constraint (1690–1545 cal yr B.P.; Table 2).

From McDaniel Creek, nine radiocarbon ages combine to provide a 1700-year chronology (Table 2). One maximum age (283–1 cal yr B.P.) from the shallowest organic-rich unit falls within the last ~300 yr radiocarbon calibration plateau. The timing of burial of the second organic-rich unit is constrained by two maximum ages (965–929 cal yr B.P. and 951–804 cal yr B.P.) and one

TABLE 2. SUMMARY OF NORTHERN HUMBOLDT BAY RADIOCARBON AGES

Calibrated age (2σ cal yr BP)*	Analytical age (1σ ^{14}C yrs BP)†	Lab number	^{13}C (‰)	Site identifier	Depth (cm)	Description of dated material	Age interpretation	Contact
Mad River Slough								
307–1	235 ± 20	OS-117742	–24.84	MR.14.02.B	140.5–141.5	Herbaceous stem	Maximum	A
511–476	420 ± 15	OS-117743	–13.89	MR.14.02.B	161.5–162.5	*Distichlis* rhizome	Maximum	B
956–802	990 ± 20	OS-117744	–11.39	MR.14.02.B	225.5–226	Two *Distichlis* rhizomes	Maximum	C
956–912	1000 ± 15	OS-119964	–26.65	MR.14.05.B	188.5–189	Herbaceous stem	Maximum	C
1057–961	1100 ± 20	OS-117822	–24.8	MR.14.02.A	273–273.5	Detrital *grindelia* stem	Minimum	D
1280–1183	1290 ± 15	OS-119965	–25.69	MR.14.05.C	246–247	Rhizome	Maximum	D
1690–1545	1690 ± 20	OS-118743	–25.57	MR.14.02.A	297.50–298.25	~25 seeds (*atriplex* and *potamogeton*)	Maximum	E
McDaniel Creek								
283–1	170 ± 15	OS-119960	–24.32	MD.14.03.C	117–118	Herbaceous stem	Maximum	A
926–798	955 ± 15	OS-119963	–25.64	MD.14.06.C	168.5–169.5	Rhizome	Minimum	C
951–804	990 ± 15	OS-117738	–26.03	MD.14.06.C	169.5–170.5	Two rhizomes	Maximum	C
965–929	1040 ± 15	OS-117739	–26.82	MD.14.03.C	212.5–213.5	Rhizome	Maximum	C
1399–1328	1480 ± 15	OS-119962	–27.84	MD.14.05.A	276–277	Rhizome and stem fragments	Maximum	D
1302-1190	1340 ± 20	OS-134119	–14.11	MD.17.13.D	250–251	Rhizome fragment	Maximum	D
1707–1575	1740 ± 15	OS-119961	–27.06	MD.14.05.B1	306.5–307.5	Herbaceous stem (detrital?)	Minimum	E
1695–1565	1720 ± 15	OS-117740	–28.02	MD.14.05.B1	308–309	Two rhizomes	Maximum	E
1708–1614	1750 ± 15	OS-117741	–15.26	MD.14.04.B	379.5–380.5	*Distichlis* rhizome	Maximum	E
Jacoby Creek								
289–1	195 ± 15	OS-117608	–13.5	JC.14.02.C	81–82	*Distichlis* rhizome	Maximum	A
1263–1082	1240 ± 20	OS-123307	–12.82	JC.14.02.D	104–105	Herbaceous stem (detrital?)	Outlier	N/A
1333–1285	1390 + 20	OS-124863	–24.62	JC.14.02.D	103–105	*Potamogeton* seed casings (detrital?)	Outlier	N/A
Modern	>Modern	OS-125075	–16.36	JC.14.02.B	100–101	Herbaceous stem (detrital?)	Outlier	N/A
1166–968	1130 ± 20	OS-119878	–26.64	JC.14.02.D	130–130.5	Rhizome	Minimum	D
1277–1181	1280 ± 20	OS-117609	–27.65	JC.14.02.C	125.5–126	Rhizome fragments	Maximum	D
1692–1561	1710 ± 15	OS-119959	–28.43	JC.14.02.C	167.5–168	Wood fragment (detrital)	Minimum	E
1694–1558	1710 ± 20	OS-117610	–27.4	JC.14.02.C	170–171.5	Rhizome or stem	Maximum	E

*Calibrated ages in calendar years before 1950 (BP) were calculated using OxCal (version 4.3.4, Bronk Ramsey [2009a]; 95% probability distribution at 2σ) with the IntCal13 dataset of Reimer et al. (2013).

†Age, calculated using a radiocarbon half-life of 5568 years and reported at one standard deviation in radiocarbon years before 1950 by the National Ocean Sciences Accelerator Mass Spectrometry Facility, Woods Hole, Massachusetts.

§Site identifier codes: MR—Mad River Slough; MD—McDaniel Creek; JC—Jacoby Creek.

minimum age (926–798 cal yr B.P.). Two ages (1302–1190 cal yr B.P. and 1399–1328 cal yr B.P.) from the third deepest organic-rich unit provide maximum age constraints of the peat unit. Due to the availability of representative stratigraphy during the initial field and dating efforts, one maximum age (1399–1328 cal yr B.P.) was taken from 15 cm below the upper contact of the unit. Two maximum ages (1708–1614 cal yr B.P. and 1695–1565 cal yr B.P.) and a minimum age (1707–1575 cal yr B.P.) tightly constrain the timing of burial of the fourth deepest organic-rich unit.

From Jacoby Creek we obtained eight radiocarbon ages from a single core (*JC.2*) that provides a 1700-year chronology (Table 2). One maximum age (289–1 cal yr B.P.) from the shallowest organic-rich unit falls within the last ~300 yr radiocarbon calibration plateau. Maximum ages were derived from the second and third buried, organic-rich units (1277–1181 cal yr B.P. and 1694–1558 cal yr B.P., respectively). Two minimum ages that may be detrital were derived from plant macrofossils found within mud units directly overlying the two deeper buried, organic-rich units (1166–968 cal yr B.P. and 1692–1561 cal yr B.P., respectively).

Also, at *JC.2* we observed a ~7-cm-thick slightly organic unit that was ~5 cm beneath the shallowest organic-rich unit (Fig. 2D). Although we did not recognize a lithological change from visual inspection in the field, a density contrast within the core was identified through CT analysis. Due to the similarity to a contact observed in two cores at Mad River Slough (*MR.2* and *MR.7*), we obtained three maximum ages for this slightly organic-rich unit (modern [post 1950 CE], 1263–1082 cal yr B.P., and 1333–1285 cal yr B.P.). Either downward root penetration, bioturbation, or contamination of the core during extraction may explain the anomalously young modern age. The two older radiocarbon ages are stratigraphically inconsistent (Table 2) with the ages from the deeper two buried, organic-rich units, possibly indicating the redeposition of older material. Therefore, we hypothesize that this contact may have been eroded at Jacoby Creek sometime prior to the 250 yr B.P. earthquake. Because these three radiocarbon ages are inconsistent with ages of the rest of the core and are not in stratigraphic order, we do not include them within the composite stratigraphy used to develop Bayesian age models.

Correlation of Stratigraphy among the Study Sites

The age results provide context for stratigraphic correlations both within the marsh as well as across the estuary. In total, we observed five mud-over-peat and/or mud-over-upland soil contacts within the tidal wetland stratigraphy at northern Humboldt Bay. However, correlation of only four submergence contacts is supported by stratigraphic mapping, depth, and radiocarbon age overlap. We assign submergence contacts with letter designations by depth, e.g., contact A is the shallowest submergence contact. We correlate three submergence contacts, e.g., A, D, and E, across all three marsh sites, contact C across two marsh sites (Mad River Slough and McDaniel Creek), and Contact B was only observed at one marsh (Mad River Slough).

Contact A

Contact A is the upper contact of the shallowest, most distinct, and most widespread buried, organic-rich unit observed at northern Humboldt Bay. Three maximum-limiting radiocarbon ages, one from each marsh, of an in-growth position rhizome and two herbaceous stems each ≤10 mm below the contact, range between 283–1 cal yr B.P. and 307–1 cal yr B.P., corroborate stratigraphic correlation across the estuary (Table 2). Contact A has radiocarbon ages consistent with previous research at Cascadia (Atwater, 1987; Nelson, 1992; Nelson et al., 1995; Satake et al., 1996, 2003; Atwater et al., 2005), which infers that the contact dates from the 250 cal yr B.P. (1700 CE) earthquake. For the remainder of the paper, we will refer to Contact A as the contact that formed due to subsidence from the 1700 CE earthquake.

Contact B

Contact B has the most limited lateral extent within the estuary because it was only observed

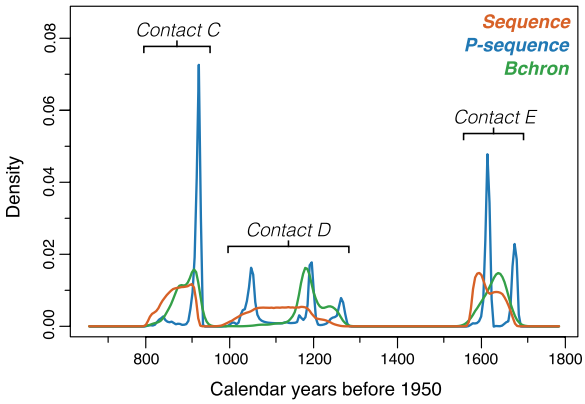

Figure 4. Alternative age models of subsidence contacts C, D, and E from northern Humboldt Bay developed using Bchron (green), OxCal Sequence (orange), and OxCal P-sequence (blue) are shown.

in cores *MR.2* and *MR.7* at Mad River Slough, which are less than 30 m apart (Fig. 2B; Table 1). At 161.5 cm and 166.5 cm core depth at *MR.2* and *MR.7*, the sharp upper contact of the organic-rich unit has ~7 mm of relief and is <10 cm below the base of the buried 1700 CE peaty unit that forms Contact A. The organic-rich unit of Contact B is 2–4 cm thick and contains 0.25–0.5-cm-thick intercalated clastic beds. The overlying 8–10-cm-thick mud unit contains ~0.25-cm-thick intercalated, slightly rooted beds. One maximum age of an in situ plant macrofossil found within 1 cm below contact B, 511–476 cal yr B.P., does not overlap with any other radiocarbon age obtained in our investigation (Table 2).

Contact C

Based on stratigraphic mapping and radiocarbon age overlap, contact C was observed at Mad River Slough and McDaniel Creek. Four maximum ages and one minimum age constrain the timing of contact C. A rhizome in growth position <10 mm above the contact at *MD.06* ranges in age from 926 cal yr B.P. to 798 cal yr B.P. (Table 2). Three rhizomes in growth position and a herbaceous stem, each within <10 mm below the contact, range in age from 956 cal yr B.P. to 802 cal yr B.P. (Table 2).

Contact D

Based on stratigraphic mapping and radiocarbon age overlap, contact D was observed at every marsh within the northern Humboldt Bay estuary. Two minimum ages and three maximum ages, one from each marsh, constrain the timing of Contact D. A *Grindelia* spp. stem <25 mm above the contact, and a rhizome in growth position <15 mm from the contact ranges in age from 1166 cal yr B.P. to 961 cal yr B.P. Three maximum age samples of a rhizome in growth position, rhizome fragments, and stem fragments were each found within 15 mm below the contact and range in age from 1399 cal yr B.P. to 1181 cal yr B.P. (Table 2).

Contact E

Based on stratigraphic mapping and radiocarbon age overlap, contact E was observed at every marsh within the northern Humboldt Bay estuary. Two minimum ages and four maximum ages of plant microfossils constrain the timing of contact E. Minimum ages of wood fragments and a herbaceous stem, both <30 mm above the contacts, have an age range of 1707–1561 cal yr B.P. One minimum age, 1707–1575 cal yr B.P., is older than three of the four maximum ages. The four maximum ages on two rhizomes in growth position, one rhizome or stem, and ~25 *Atriplex* and *Potamogeton* seeds <20 mm below the contact have a combined age range of 1708–1558 cal yr B.P. (Table 2).

Modeling the Timing of Abrupt Submergence

We constructed a representative composite stratigraphic section using 16 radiocarbon ages across the estuary (Fig. S1[1]). Ages were assigned to appropriate depth intervals relative to the upper contact of buried, organic-rich units that were stratigraphically widespread: contacts A, C, D, and E. The composite stratigraphy was based on the stratigraphy observed at *MD.5* (Figs. 2C and 3A), where contacts A, C, D, and E were described at the depths of 126 cm, 173 cm, 246 cm, and 312 cm from the surface, respectively (Fig. S2). We do not model contact B or include the maximum age constraint obtained at this contact within the composite stratigraphy because of a lack of correlative stratigraphy at McDaniel Creek to allow its placement onto the composite stratigraphic section. We do not model contact A due to the limitations of radiocarbon imposed by a plateau in the calibration curve post 1650 CE (Reimer et al., 2013). The assumption that contact A represents the Cascadia subduction zone 1700 CE megathrust earthquake is consistent with the tsunami modeling of Satake et al. (1996) and Satake et al. (2003), tree ring ages from Nelson et al. (1995), reservoir-corrected offshore ages of foraminifera that are not subject to the radiocarbon calibration plateau (Goldfinger et al., 2012, 2013), and our three maximum limiting radiocarbon ages of contact A (Fig. 3 and Table 2).

The estuary-wide composite stratigraphy (Fig. S1), based on the stratigraphy observed at *MD.5* (Figs. 1 and 2), was used in the construction of the three Bayesian age models (Fig. 4). We employ the OxCal Sequence as a simple Bayesian age model using stratigraphic position to order ages as well as the more complicated OxCal P-sequence and Bchron age models, which incorporate depths and variable sedimentation rates, to develop paleoseismic chronologies at northern Humboldt Bay and evaluate the effect that model and software choices have on our results (Figs. S1–S7; see footnote 1).

In general, each of the Bayesian age models shows strong agreement on the timing of burial of each of the modeled contacts (Fig. 4; Table 3). For contacts C, D, and E, the variability of modeled mean ages range over 38 years, 25 years, and 19 years, respectively (Table 3). For contacts C and D, Bchron provides narrower age ranges than the OxCal Sequence and P-sequence models, which is the result of the model-assigned sedimentation rate between age constraints.

[1]Supplemental Material. Tables S1–S32 and Figures S1–S7. Please visit https://doi.org/10.1130/GSAB.S.13377062 to access the supplemental material, and contact editing@geosociety.org with any questions.

TABLE 3. SUMMARY OF BAYESIAN AGE MODELS

Contact	OxCal 4.2 Sequence calibrated age (yr B.P.)					OxCal 4.2 P_Sequence calibrated age (yr B.P.)					Bchron calibrated age (yr B.P.)				
	From	To	μ	σ	m	From	To	μ	σ	m	From	To	μ	σ	m
C	924	816	874	30	877	935	825	905	24	917	939	845	867	47	880
D	1231	1004	1117	61	1118	1280	1003	1139	85	1165	1273	1133	1142	96	1145
E	1669	1575	1618	28	1615	1693	1595	1637	32	1620	1682	1587	1630	59	1625

Notes: μ—mean; σ—one standard deviation; m—mode.

For contact E, all modeled mean age ranges are essentially identical (within four years; Fig. 4; Table 3). The tight age overlap of the contact E result is likely based on the combination of (1) the narrow radiocarbon age range of 147 years between the youngest minimum (1692–1561 cal yr B.P.) and oldest maximum (1708–1614 cal yr B.P.) and (2) the close depth distribution of our age constraints, i.e., two minimum ages within the first <3 cm above the contact and four maximum ages within the first 2 cm below the contact (Fig. 3; Table 2; and Fig. S1).

For each modeled contact age, the OxCal P-sequence age model produces broader age ranges than the OxCal Sequence and Bchron models. The relatively broad age range results may be attributed to the assigned *k* value. For the northern Humboldt Bay chronologic data and following Bronk Ramsey (2008) and Enkin et al. (2013), we determined that the optimal *k* is 0.1 cm^{-1}, meaning that variations in deposition rate occur on average about every 0.1 cm (Table 2; Tables S1–S28; Figs. S1–S2). A large *k* value directs a more uniform sedimentation rate (Bronk Ramsey, 2008), which can over-constrain the age model (i.e., produce narrower age ranges) and result in low agreement indices (Enkin et al., 2013; Tables S1 and S15–S28). In contrast, a small *k* value allows for a greater randomness in the deposition rate and weights superposition of samples over sample depth (Bronk Ramsey, 2008), which results in less constrained age ranges (i.e., wider age ranges) and high agreement indices (Enkin et al., 2013; Tables S1–S14). Therefore, when *k* is small and radiocarbon age constraints are clustered around contacts of interest, OxCal P-sequence models more conservative age ranges (Table 3; Fig. 4; Figs. S4–S6). For example, the timing of burial for contact D is constrained by 309 years between the oldest minimum limiting age (1166–968 cal yr B.P.) and youngest maximum limiting age (1277–1181 cal yr B.P.); the more conservative OxCal P-sequence-modeled age for contact D has the largest range of 277 years, whereas OxCal Sequence and Bchron model less conservative age ranges of 227 years and 140 years, respectively (Table 3).

Foraminiferal Analyses Across Submergence Contacts

We selected representative sediment cores for foraminiferal analyses from McDaniel Creek because it archives the largest lateral extent of contacts A, C, D, and E (Fig. 5; Tables S29–S33 [see footnote 1]). Further, we analyzed contact B from Mad River Slough due to the absence of this contact at McDaniel Creek and Jacoby Creek to identify whether it may be related to a subduction zone earthquake (Table S30). Sudden and lasting foraminiferal community assemblage changes were found across four abrupt-to-sharp contacts: A, C, D, and E (Fig. 5; Tables S29 and S31–S33). We did not apply the BTF to the fossil data across contact B because change was only minimal in fossil foraminiferal assemblages between the organic-rich unit and the overlying clastic mud (Table S30). The BTF results show that contact A and contact D record a similar amount of subsidence, contact C archives the smallest amount of subsidence, and contact E records the largest magnitude of subsidence. Pairwise comparison of modern and fossil foraminiferal assemblages were well below the 20th percentile threshold, which indicates that all fossil assemblages had modern analogs.

For contacts A, C, D, and E, we first describe the lithology around the representative contact and then provide a description of the foraminiferal biostratigraphy.

Contact A

At *MD.03*, the shallowest buried, organic-rich unit abrupt upper contact is at 115 cm core depth (Fig. 5A). The organic-rich brown peat unit is 8 cm thick and capped by a gray mud that extends >25 cm. The CT scan of *MD.3* shows an abrupt 1–2 mm contact with ~5 mm of relief and fine bedding within the overlying mud unit from 97 cm to 115 cm core depth indicated by alternating yellow and orange layers (Fig. 5A) that represent differing densities of sediment.

Foraminiferal assemblages in the brown peat unit are dominated by *B. pseudomacrescens* (27%–54%), *T. inflata* (7%–39%), and *J. macrescens* (5%–33%), which is consistent with a MHHW salt marsh environment. Samples in the mud overlying the peat unit show an increase in the abundance of *M. fusca* (5–14%), *Reophax* spp. (0.05%–3%), *Ammobaculites* spp. (0%–1.4%), and *J. macrescens* (25–54%) and a decrease in the abundance of *B. pseudomacrescens* (12–29%) and *T. inflata* (16–27%). The presence of *Ammobaculites* spp., *Reophax* spp., and the increase of *M. fusca* is consistent with a tidal flat environment near MTL (Fig. 4; Kemp et al., 2018). The fossil foraminifera BTF reconstruction suggests 0.85 ± 0.46 m of subsidence (Fig. 5A; Table 4; Table S29).

Contact B

At *MR.2*, we found no distinct change in foraminiferal assemblages across contact B (Table S30). The organic-rich unit fossil assemblages are primarily composed of *B. pseudomacrescens* (38%–49%), *J. macrescens* (23%–32%), *T. inflata* (16%–20%), and *M. fusca* (0%–1%), which is consistent with a peat soil forming near MHHW. Although samples in the mud overlying the peat unit show a slight increase in the abundance of *M. fusca* (2%–3%), *Reophax* spp. (0%–1%), and *T. inflata* (22%–25%), the moderate to high abundances of *B. pseudomacrescens* (38%–41%) and *J. macrescens* (21%–29%) are also consistent with an environment forming between MHW and MHHW (Table S30).

Based on a lack of lateral extent of the contact, lack of radiocarbon age overlap within the estuary, and minimal fossil foraminiferal assemblage change, we do not apply the BTF to the fossil foraminifera assemblage data from contact B and we infer that it does not represent coseismic subsidence induced from megathrust rupture. Instead, we infer that this organic-rich unit is the base of the organic-rich unit below contact A and that the 8–10-cm-thick mud that separates these organic-rich units could be a local hydrographic event; a possible cause is an overtopping of the Mad River levee that is 6 km to the north-northeast.

Contact C

At *MR.6*, the upper contact of the second deepest buried, organic-rich unit at 170.5 cm core depth is sharp and separates a muddy peat from an overlying mud (Fig. 5B). The brown muddy peat unit is 6 cm thick and capped by a gray mud that extends >20 cm. CT images show a sharp ~3 mm contact with ~5 mm of undulating relief and >6 cm of overlying mud that contains detrital organics and/or paleoburrow. The semi-vertical void that extends across the CT image is possibly a crack that occurred during sediment collection and/or shipping (Fig. 5B).

Foraminifera in the light brown muddy peat unit dominantly consist of *B. pseudomacrescens* (12%–40%) and *T. inflata* (24%–36%), both of which are consistent with a MHHW salt marsh environment. Samples in the gray mud overlying the peat unit show an increase in the abundance of *M. fusca* (21–33%) and *J. macrescens* (27–37%) and a decrease in the abundance of *B. pseudomacrescens* (4–9%), which is consistent with an environment below but in close proximity to MHW. The fossil foraminifera BTF reconstruction shows 0.42 ± 0.37 m of subsidence (Fig. 5B; Table 4, Table S31).

Contact D

The CT scan of *MD.13* shows a sharp contact at 248 cm to have ~14 mm of undulating relief and separates an 8-cm-thick organic-rich unit, where the upper 3 cm are a light brown muddy peat and the lower 5 cm are a gray-brown rooted mud, from a >25-cm-thick finely bedded gray mud.

Foraminifera in the organic-rich unit dominantly consist of *B. pseudomacrescens* (3%–48%), *T. inflata* (9%–71%), and *J. macrescens* (22%–52%), which is consistent with a MHHW salt marsh environment. Although samples in the gray mud overlying the peat unit are also

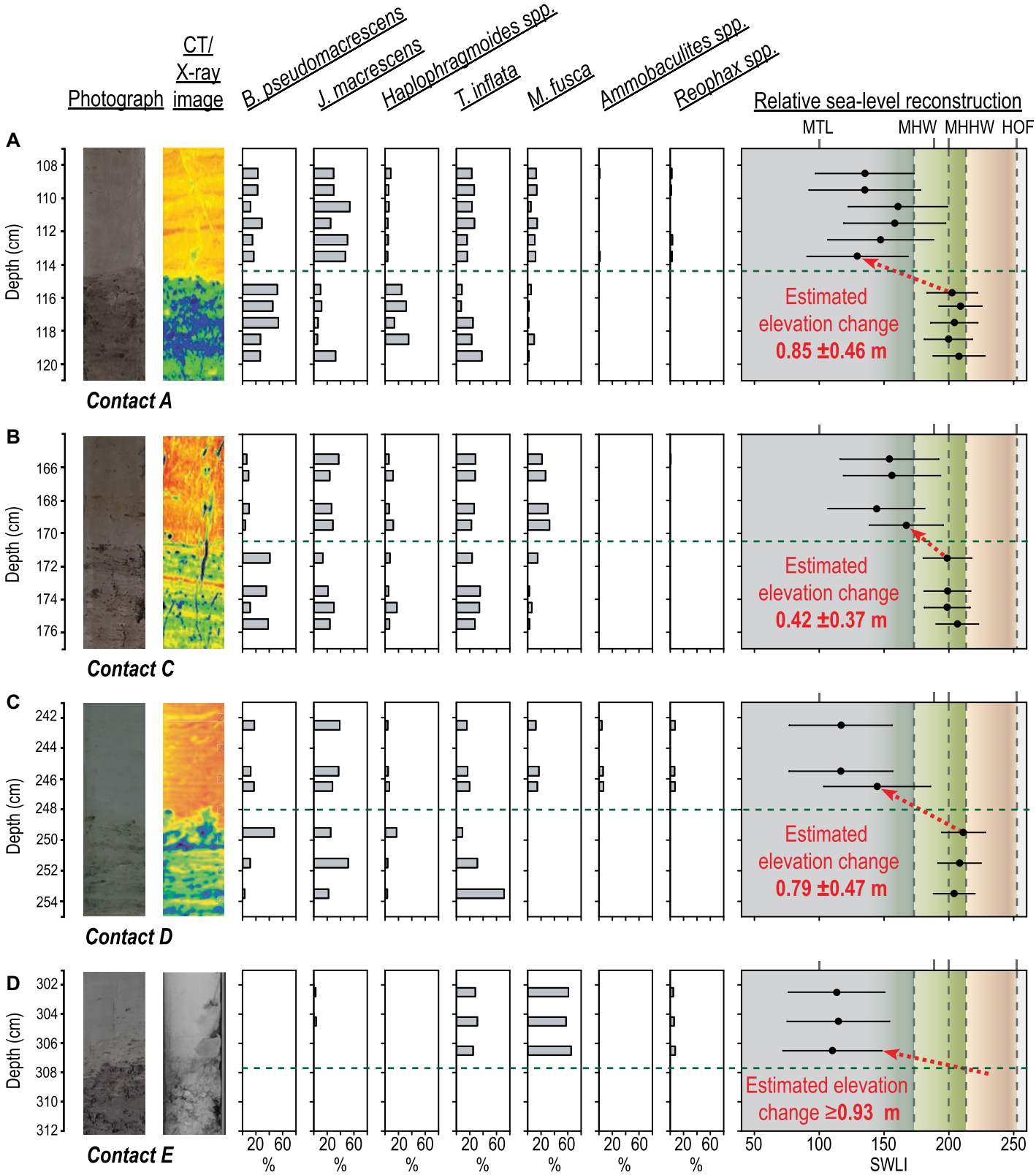

Figure 5. Plots showing McDaniel Creek stratigraphy for four contacts: (A) Contact A at *MD.3*, (B) Contact C at *MD.6*, (C) Contact D at *MD.13*, and (D) Contact E at *MD.5*. The plots include photo images, computerized tomography (CT) scans (rainbow scale; warm colors—more dense and cool colors—less dense), percent foraminifera (gray bar), and results of Bayesian transfer function-reconstructed sea level with error bars that represent 1σ uncertainties. HOF—highest occurrence of foraminifera; SWLI—sea water level index; MTL—mean tide level; MHW—mean high water; MHHW—mean higher high water.

TABLE 4. SUMMARY OF SUBSIDENCE ESTIMATES

Contact	Core site	Depth of contact (cm)	Subsidence estimate (m)
A	MD.3	115	0.85 ± 0.46
C	MD.6	170	0.42 ± 0.37
D	MD.13	222	0.79 ± 0.47
E	MD.5	307	≥ 0.93

dominated by *J. macrescens* (27%–38%), *T. inflata* (15%–19%), and *B. pseudomacrescens* (12%–18%), the assemblages show a marked increase in the abundance of *M. fusca* (14–17%) and contain *Ammobaculites* spp. (~1%) and *Reophax* spp. (~1%), which are typically associated with a tidal flat environment near MTL (Kemp et al., 2018). For the subsidence estimate we use the distributions of the reconstructed RSL elevations that are 2 cm apart and are the first unmixed centimeter intervals above and below the mud-over-peat contact. The fossil foraminifera BTF reconstruction shows 0.79 ± 0.47 m of subsidence across contact D (Fig. 5C; Table 4; Table S32).

Contact E

At *MD.5*, the sharp upper contact of the deepest buried, organic-rich unit is at 308 cm depth, undulates over >15 mm, and separates a dark gray-black, organic-rich unit from an overlying gray mud (Fig. 5D). The organic-rich unit is 12 cm thick and is overlain by a gray mud that extends thicker than 25 cm. X-ray analysis shows that the overlying gray mud infiltrated into the underlying highly humified and friable organic-rich unit below (Fig. 5D).

The fossil foraminifera assemblages further support the interpretation of mixing across contact E. The foraminifera assemblages in the humified, organic-rich unit have decreasing abundances, from 200 to <30, with 4 cm distance below the contact. The humified organic-rich unit is dominated by *M. fusca* (48%–52%), *T. inflata* (35%–38%) and contains low abundances of *Reophax* spp. (<1%); such an assemblage is typically indicative of an environment that formed below MHW. However, while foraminifera abundances above the deepest organic-rich unit are consistent with other analyzed intervals (>200 individuals) the decreasing abundances of foraminifera with distance from the upper contact of the organic-rich unit is consistent with mixing (e.g., Engelhart et al., 2013a; Milker et al., 2015). Based on visual appearances in photos and X-ray imagery, decreasing foraminiferal abundances, and similarity to foraminiferal assemblages within the overlying clastic mud unit, we interpret that foraminifera assemblages found within the organic-rich unit are not in situ or indicative of the depositional environment. Moreover, Engelhart et al. (2016) report diatom analysis of core *JC.14.02A* at Jacoby Creek that suggests the organic-rich unit formed as a dry upland surface and not as salt marsh. Therefore, considering the diatom data at *JC.14.02A,* correlation of radiocarbon ages, and a lack of in situ fossil foraminiferal assemblages, we conclude that the fourth deepest organic-rich unit represents a depositional environment that formed above the highest occurrence of foraminifera. Foraminifera in the gray mud above the organic-rich unit are dominated by *M. fusca* (60%–65%) and *T. inflata* (25%–31%), while *Ammobaculites* spp. and *Reophax* spp. are both present at ~1%, signifying an assemblage that formed at around MTL. Based on the first interval that contains in situ fossil foraminifera above the organic-rich unit, we subtract the reconstructed RSL elevation for this interval, as predicted by the BTF, from the elevation of the highest occurrence of foraminifera in northern Humboldt Bay, which is 2.5 m (NAVD 88). Therefore, fossil foraminifera assemblages can only provide a minimum-limiting estimate for subsidence of ≥ 0.93 m (Fig. 5B; Table 4; Table S33).

DISCUSSION

We provide multiple lines of evidence for four megathrust earthquakes since 1700 cal yr B.P. in northern Humboldt Bay (Table 5). These results prompt important questions, introduced above, about age modeling techniques that best constrain the ages of past subduction zone earthquakes and questions about needed levels of resolution in both the chronology of paleoearthquakes and the amount of coseismic subsidence during paleoearthquakes such that individual paleoearthquakes can be correlated along the Cascadia margin. Next we address the questions in the context of the northern Humboldt Bay tidal wetland stratigraphic record and compare the northern Humboldt Bay paleoearthquake record to other regional paleoseismic sites and consider the possibility of correlating variable subsidence data for different earthquakes among sites in southern Cascadia.

Northern Humboldt Bay Paleo Subduction Zone Earthquake Record

Revisions to the Tidal Wetland Stratigraphy in Northern Humboldt Bay

Our new lithologic, biostratigraphic, and chronologic analyses allow us to provide a refined paleoseismic history of subduction zone earthquakes for northern Humboldt Bay. Tidal wetland stratigraphic records are a proven means for reconstructing paleoearthquakes at subduction zones globally. The records of mud-over-peat and mud-over-upland soil contacts are convincing lines of evidence for land subsidence induced by great ($M > 8$) and giant ($M > 9$) earthquakes (e.g., Atwater, 1987). However, since the stratigraphic record at Cascadia was initially linked to such earthquakes (e.g., Atwater, 1987; Darienzo and Peterson, 1990; Atwater and Yamaguchi, 1991; Atwater, 1992; Nelson, 1992), continued focus on other processes that may cause stratigraphy similar to coseismic subsidence (Long and Shennan, 1994; Allen, 1997, 2000; Nelson et al., 1998) has led to the development of the rigorous stratigraphic research framework that underpins modern coastal subduction zone paleoseismology (Nelson et al., 1996a; Shennan et al., 2016). Many of the foundational tidal wetland stratigraphic papers for northern Humboldt Bay preceded the development of this framework (e.g., Vick, 1988; Clarke and Carver 1992; Valentine, 1992) so that even later review articles (e.g., Valentine et al., 2012) may not adequately represent the uncertainty in the tidal wetland stratigraphy mapped at different sites by different researchers.

This uncertainty is highlighted by the complicated stratigraphy at Mad River Slough, specifically a contact observed by previous researchers that we refer to as contact B (e.g., Vick, 1988; Clarke and Carver 1992; Valentine, 1992; Valentine et al., 2012). Previous research was not able to conclude if contact B represents megathrust-induced coseismic subsidence because of

TABLE 5. BURIED, ORGANIC-RICH UNIT ATTRIBUTES CONSISTENT WITH SUBDUCTION EARTHQUAKE ORIGIN

Contact	Sharp (<3 mm) contact between buried, organic-rich unit and overlying mud	Long-lasting relative sea-level rise (overlying mud >10 cm thick)	Fine to very fine sand layer immediately overlies submergence contact	Foraminifera assemblages consistent with abrupt relative sea-level rise across contact	The contact is laterally extensive, e.g., observed across estuary	Calibrated age range (2σ) of buried, organic-rich unit is chronologically consistent with regional record of Cascadia subduction zone earthquakes
A	✓	✓		✓	✓	✓
B	✓					
C	✓	✓		✓	~✓	✓
D	✓	✓		✓	✓	✓
E	✓	✓		✓	✓	✓

~ Not observed at Jacoby Creek.

the limited spatial extent of the contact (contact B is observed only at MRS-3 core location of Vick, 1988), the lack of radiocarbon age correlation within the estuary (Clarke and Carver, 1992; Valentine, 1992; Valentine et al., 2012), and limited qualitative microfossil analysis (Valentine et al., 2012). Additionally, even though Pritchard (2004) reoccupied several core and outcrop stratigraphic description locations of previous researchers (e.g., Clarke and Carver, 1992; Valentine, 1992; Valentine et al., 2012), including MRS-3 of Vick (1988), contact B was not included within their stratigraphic descriptions. Moreover, several previous researchers correlate contact B with evidence from other proximate paleoseismic wetland stratigraphic and trench investigations (e.g., Clarke and Carver, 1992; Valentine, 1992; Valentine et al., 2012). We contend that across-site/estuary correlations based on the relatively large error range of radiocarbon ages of bulk peat samples (e.g., Clarke and Carver, 1992; Valentine et al., 2012), relative order inferences placed on narrowly supported hypothetical composite stratigraphic sections (e.g., fig. 16 of Valentine, 1992; Valentine et al., 2012), and a lack of within-site radiocarbon age replications (e.g., Clarke and Carver, 1992; Valentine, 1992; Valentine et al., 2012) provide insufficient evidence for correlation beyond a small area of marsh in a single, potentially complicated stratigraphic section. Therefore, differing stratigraphic observations and limited radiocarbon age constraints are primarily responsible for the previous, divergent correlations and conclusions of paleoseismic investigations of northern Humboldt Bay.

However, our extended stratigraphic descriptions (Figs. 2 and 3 and Table 1) and robust radiocarbon data set (Table 2) from new coring at McDaniel Creek and Jacoby Creek allow us to provide further clarification. Our new results do not provide any additional evidence for a contact of the age of contact B at other northern Humboldt Bay sites. Instead, we suggest that contact B is likely the result of a simpler explanation of physical processes within Mad River Slough and could be related to the overtopping of the Mad River levee during an unusual flood event (Cahoon et al., 1996; Friedrichs and Perry, 2001), local marsh-edge slumping (Allen, 1989; Gabet, 1998), or soil creep (Mariotti et al., 2016), which could all potentially create non-seismic induced submergence-like stratigraphy over small spatial scales (Nelson et al., 1996a, 2006; Shennan et al., 2016). Barring further evidence from additional sites within northern Humboldt Bay, based solely on our observations we suggest that contact B is not representative of a Cascadia subduction zone megathrust-induced subsidence.

However, we acknowledge that the maximum ages derived from the organic-rich unit below contact B overlap with the age of the T2 turbidite (Goldfinger et al., 2012). Subsidence lesser than the threshold required to record it consistently in the salt-marsh sediments across northern Humboldt Bay (e.g., Nelson et al., 1996a; Shennan et al., 2016) could possibly be invoked to correlate this very sparse record with T2. Nonetheless, the currently available coastal observations, limited spatial evidence for contact B, and a lack of foraminiferal assemblage change across contact B (Table S30) favor other local processes over megathrust-induced subsidence.

Greater confidence can now be assigned given our estuary-wide stratigraphic correlations based on (1) an increase in the spatial density and extent of stratigraphic descriptions beyond those from previous northern Humboldt Bay paleoseismic investigations (i.e., at McDaniel Creek and Jacoby Creek sites) and (2) our robust radiocarbon age data set, which elucidates stratigraphic correlations throughout the estuary (Tables 1 and 2). At northern Humboldt Bay, four stratigraphic contacts meet the criteria (Hemphill-Haley, 1995; Nelson et al., 1996a; Shennan et al., 2016) for coseismic subsidence: contacts A, C, D, and E (Table 5). This result is consistent with portions of the findings from previous research (Vick, 1988; Clarke and Carver, 1992; Valentine, 1992; Pritchard, 2004; Valentine et al., 2012). Based on our stratigraphic mapping and radiocarbon ages, McDaniel Creek archives the most consistent wetland stratigraphic record of Cascadia subduction zone rupture in north Humboldt Bay (Figs. 2 and 3). This is in contrast to previous research that has focused on Mad River Slough as the type section in northern Humboldt Bay (Vick, 1988; Clarke and Carver, 1992; Valentine, 1992; Valentine et al., 2012). We contend that due to inconsistent and variable stratigraphy and the potential influence of slough processes (e.g., Nelson et al., 1998), the Mad River Slough stratigraphic record should be treated with caution.

Radiocarbon Age Modeling of Southern Cascadia Earthquake Chronology: Advantages and Disadvantages of Alternative Bayesian Age Models

Our work refining the northern Humboldt Bay radiocarbon data set and constructing Bayesian age models (Fig. 4 and Table 3) provides opportunity for testing, calibrating, and refining chronologic models. We move beyond traditional radiocarbon-based dating approaches by assessing the results of multiple Bayesian age models, which may improve the accuracy and precision of earthquake chronologies. For earthquakes prior to 1700 CE, even the most conservative age model (OxCal Sequence) provides narrower age distributions (age ranges of between 94 years and 227 years) than previous paleoseismic investigations at northern Humboldt Bay (e.g., Vick, 1988; Clarke and Carver, 1992; Valentine, 1992; Valentine et al., 2012): 924–816 cal yr B.P., 1231–1004 cal yr B.P., and 1669–1575 cal yr B.P. (Table 3). The timing of earthquakes may be refined further by incorporating modeled sedimentation rates between radiocarbon age (OxCal P-sequence and Bchron models).

We select an age model that ignores sedimentation rate for three reasons. Despite the often-narrower age distributions provided by Bchron (which incorporates sedimentation rates), the OxCal Sequence age estimates are the most reliable for the paleoseismic activity at northern Humboldt Bay. First, if the age constraints above (minimum age) and below (maximum age) a contact of interest are derived close (e.g., $\sim$<3–4 cm) to the contact of interest and have considerable age range overlaps, then each of the three Bayesian models we tested provides nearly identical age estimates, e.g., contact E (Table 3). Therefore, a modeled sedimentation rate does not always improve the modeled age estimate if the data constraints are consistent. Second, our radiocarbon data set cannot resolve the variations in post-seismic sedimentation in the northern Humboldt Bay wetlands. Near Portage, Alaska, Atwater et al. (2001) document environmental changes over three decades after the great 1964 Alaska earthquake. Sedimentation was rapid within the first several months and then slowed in the decades following as the previous vegetation and environments re-established (Atwater et al., 2001). Therefore, post-seismic variable sedimentation rates likely vary over timeframes less than the uncertainty of radiocarbon ages. Unlike the use in passive margins of sedimentation rate-informed age models, where sedimentation rates are likely to be more consistent (e.g., Kemp et al., 2009, 2011; Wright et al., 2017), care should be taken in active margins when constructing age models that perhaps unwittingly are modeling an uncertain and variable sedimentation rate. Third, the development of a composite stratigraphy (multiple age constraints derived from multiple cores) requires that stratigraphic correlations are accurate and stratigraphic position (depth) assignments are representative for the study site. Although radiocarbon age overlap can provide confidence in stratigraphic correlation, sedimentation/accumulation rates and erosional histories are not consistent throughout an entire wetland environment (Letzsch and Frey, 1980; Allen, 2000). Differences in sedimentation rates will affect the modeled age estimates (e.g., Tables S1–S28 and Figs. S1 and S3–S5), and combining chronologic constraints into a composite chronology (e.g., Fig. S2) assumes

that the differences in sedimentation/accumulation rates are negligible. By selecting an age model that does not model a sedimentation rate, we avoid this potential error.

Although finding a single representative core location that has abundant quality dating material (e.g., in situ plant macrofossils and/or seeds) is problematic, future research should consider acquiring dates from within a single core where possible. This approach would circumvent the need to build composite chronologies and allow greater confidence in testing the applicability of modeled sedimentation rates to constrain the timing of earthquakes at Cascadia. Additional dates from adjacent core sites could be used to verify stratigraphic correlations.

Correlating the Northern Humboldt Bay Earthquake Record to Other Paleoseismic Records on the Southern Cascadia Subduction Zone

Northern Humboldt Bay may have experienced both full and partial ruptures over the late Holocene (e.g., Goldfinger et al., 2012). Our AMS radiocarbon ages provide an unambiguous chronology for earthquake-induced subsidence at northern Humboldt Bay even without Bayesian age modeling. The precision of the conservative OxCal Sequence age model tightly constrains the timing of earthquake subsidence (Fig. 4; Table 3) and allows for increased confidence in correlation over 10–100 km (Fig. 6). This refined chronostratigraphic approach provides a means with which to test the interpretation of varying rupture length along strike. In testing models for subduction zone ruptures, we anticipate that sites close together should show the same or similar coseismic inference (Shennan et al., 2016). Therefore, we examine regional southern Cascadia paleoseismic records and correlate age overlap with the paleoseismic chronology at northern Humboldt Bay for earthquake contacts C, D, and E (Fig. 6). We also highlight age estimate overlap and offer plausible explanations for the lack of age estimate overlap when appropriate.

Earthquake Contact C, ca. 875 cal yr B.P.

Although the OxCal "Sequence" model age distribution for contact C overlaps with age ranges of plate-boundary evidence at Talbot Creek, Bradley Lake, Eel River, and the timing of turbidite T3, correlation is lacking at Coquille River, Lagoon Creek, and southern Humboldt Bay (Fig. 6). The southern Humboldt Bay site (Patton, 2004) contains earthquake evidence below the inferred Cascadia subduction zone 1700 CE contact and above a deeper and older buried, organic-rich unit upper contact. Therefore, the undated contact at southern Humboldt Bay could potentially contain a correlative age distribution with contact C at northern Humboldt Bay. At Lagoon Creek, no tsunami deposit is found with an age distribution that overlaps with contact C (Abramson, 1998; Garrison-Laney, 1998). This may be explained by foredune sequence heights that were sufficiently high to present a barrier to tsunami inundation, although why that should be an issue for this event and not others is unclear. Another potential explanation may be that because the age of

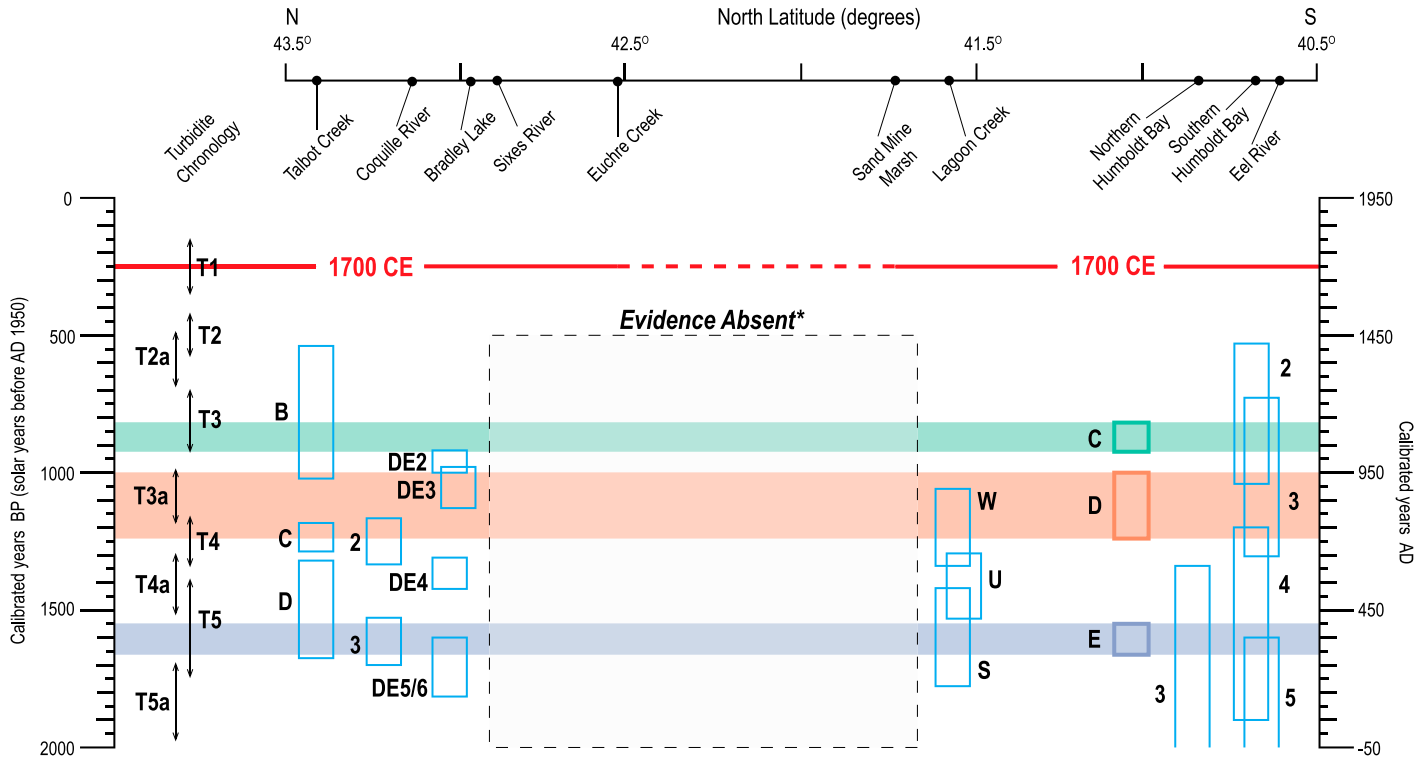

Figure 6. Comparison of dated mud-over-peat and mud-over-upland soil contacts beneath southern Cascadia salt marshes (Talbot Creek: Milker et al., 2016; Coquille River: Witter et al., 2003; Southern Humboldt Bay: Patton, 2004; Eel River: Li, 1992) and tsunami deposits at Lagoon Creek (Abramson, 1998; Garrison-Laney, 1998) and Bradley Lake (Kelsey et al., 2005) are shown with OxCal Sequence-modeled timing of subsidence contacts for northern Humboldt Bay and ages of marine turbidites (vertical black arrows show 2σ uncertainties from Goldfinger et al., 2012). *Evidence Absent—To date, evidence of coseismic subsidence in the time range ca. 500–2000 yr B.P. has not been found in the latitude range 41.7°–42.9°N. Absence of evidence may be because megathrust slip was insufficient to cause vertical deformation to be recorded by the salt marsh and/or because vertical deformation was further offshore and only minimal vertical deformation occurred at coastal sites. Further field work in salt marshes may reveal subsidence stratigraphy for the time and latitude range above.**

tsunami deposit W at Lagoon Creek is derived from detrital material, the age may not represent a close maximum age.

A lack of correlation with contact C and evidence at Coquille River (Witter et al., 2003) can be potentially explained by: (1) no earthquake occurrence at Coquille River; (2) formation threshold, where slip on the megathrust was insufficient to cause enough vertical deformation to be recorded by the salt marsh; and (3) preservation threshold, where the coastal system had not fully recovered/reset from the previous earthquake rupture at ca. 1170–1370 cal yr B.P. (e.g., Benson et al., 2001). A preservation threshold seems an unlikely cause in that there were >200 years between the previously documented earthquake and our inferred timing for contact C (Witter et al., 2003). There are correlative age distributions farther north at Talbot Creek (Fig. 6), southern Washington, and Vancouver Island (Nelson et al., 2006) and also to the south at Eel River (Fig. 6). However, at Talbot Creek, Milker et al. (2016) report little to no subsidence across their correlative contact B, and northern Humboldt Bay contact C also records the least amount of subsidence over the four most recent earthquake cycles. Minimal subsidence at the above two sites does support the inference of insufficient coseismic deformation (i.e., formation threshold) at the Coquille River during the earthquake that caused the formation of contact C. Moreover, the turbidite evidence for T3 suggests a margin-wide megathrust rupture with a relatively large mass and bed thickness at numerous sites (Goldfinger et al., 2012, 2013) could imply that the majority of slip was shallow and farther offshore, potentially limiting the creation and preservation of onshore evidence during this event in southern Cascadia.

Earthquake Contact D, ca. 1120 cal yr B.P.

The OxCal Sequence model age distribution for contact D overlaps with age ranges for evidence of plate-boundary earthquakes at Eel River, Lagoon Creek, Bradley Lake, Coquille River, Talbot Creek, and the T3a and T4 turbidites. There is no correlation with southern Humboldt Bay (Fig. 6). Although southern Humboldt Bay (Patton, 2004) contains an undated buried, organic-rich unit that could potentially correlate with either contact C or D at northern Humboldt Bay, the undated unit cannot correlate to both.

Therefore, a preservation threshold not being met is the most likely explanation for the lack of stratigraphic evidence for a plate-boundary earthquake at southern Humboldt Bay during the earthquake that caused the burial of contact D at northern Humboldt Bay. Southern Humboldt Bay may not have fully recovered/reset from the previous earthquake rupture (i.e., preservation threshold), because the age of the upper contact of buried soil 3 is estimated to be 1350–2150 cal yr B.P. (Patton, 2004), which is potentially <200 years prior to the age of contact D (Fig. 6). Although a heterogenous slip distribution and/or an insufficient amount of coseismic deformation (i.e., formation threshold) could explain the lack of stratigraphic record at southern Humboldt Bay, such an explanation seems unlikely because we estimate 0.79 ± 0.47 m of subsidence ~20 km away. Additionally, a "no earthquake occurrence" explanation also seems unlikely because there are correlative ages of stratigraphic evidence for plate-boundary rupture both to the north, e.g., Talbot Creek and Coquille River, and to the south at Eel River as well as corresponding age distributions for tsunami deposits at Bradley Lake and Lagoon Creek. Moreover, Goldfinger et al. (2012) suggest that the earthquake that caused T4 was a full-margin rupture, and the earthquake that caused T3a turbidite was a southern Cascadia rupture that extended for 444 km and encompasses basins offshore of all sites south of 43°N (Fig. 6).

Earthquake Contact E, ca. 1620 cal yr B.P.

All seven onshore sites (Fig. 6) record evidence for a plate-boundary earthquake, and the offshore turbidite T5 ages overlap with the age distribution for contact E. There are abundant corresponding age distributions for contact E offshore, throughout southern Cascadia (Fig. 6), and farther north along the Cascadia margin including central Oregon and southern Washington (Darienzo et al., 1994; Nelson et al., 1996b; Shennan et al., 1996; Nelson et al., 1998, 2004; Atwater et al., 2003; Graehl et al., 2015).

Summary: Southern Cascadia Subduction Zone Ruptured all at Once in Each of the Four Earthquakes Recorded at Humboldt Bay

In summary, in examining the paleoseismic chronology at northern Humboldt Bay for earthquake contacts C, D, and E, we document age overlap with earthquakes at the other six paleoseismic sites northward from the Eel River estuary to South Slough, an along-margin distance of ~310 km (Fig. 6). The exceptions are the ca. 875 cal yr B.P. earthquake that is not recorded at southern Humboldt Bay and Coquille River and the ca. 1120 cal yr B.P. earthquake that is not recorded at southern Humboldt Bay. Given that preservation threshold (i.e., the system had not fully recovered/reset from the previous earthquake rupture) is a reasonable justification for why these two sites do not have complete overlap of earthquake records, we infer that the southern Cascadia margin, at least from the Eel River estuary north to South Slough, could rupture all at once in each of the four subduction zone earthquakes that we document at northern Humboldt Bay. Our inference leaves open the possibility that all of the earthquakes recorded in northern Humboldt Bay may also be full-margin ruptures.

Implications for Understanding Spatial and Temporal Variability in Subsidence Amounts at Cascadia

Expanding the 1700 CE Subsidence Record

Our BTF coseismic subsidence estimate, 0.85 ± 0.46 cm (Fig. 5; Table 4), extends the latitudinal range of foraminifera-based transfer function estimates for the 1700 CE earthquake (Hawkes et al., 2010, 2011; Wang et al., 2013; Milker et al., 2016; Kemp et al., 2018). Additionally, our 1700 CE coseismic subsidence estimate is consistent with both the "preferred" model of Wang et al. (2013) and a previous subsidence estimate based on diatom analysis at Mad River Slough of 0–1.64 m (Pritchard, 2004), although with a significant improvement in precision. An increase in the density of coseismic subsidence estimates from the southern Cascadia coastline will improve knowledge of a highly complicated and dynamic region of the margin (Goldfinger et al., 2012; Wang et al., 2013; Kemp et al., 2018).

Given the spatial variation observed elsewhere in Cascadia for 1700 CE (Kemp et al., 2018), investigating the degree of spatial variation along the southern Cascadia region is appropriate. For example, the Coquille River and northern Humboldt Bay are separated by ~275 km along strike and in between several coastal paleoseismic sites do not have quantitative microfossil RSL reconstructions despite potentially containing suitable environments. North of our study site, subsidence stratigraphy of the Cascadia subduction zone 1700 CE earthquake may exist at Euchre Creek (~42.55°N; Witter et al., 2001) and Sand Mine Marsh (~41.74°N; Peterson et al., 2011; Hemphill-Haley et al., 2019), although the prospect remains uncertain. To the south of our study site, the potential for developing subsidence estimates at southern Humboldt Bay (~40.69°N; Patton, 2004) and at the mouth of the Eel River (~40.62°N; Li, 1992) would further supplement the Cascadia subduction zone 1700 CE paleogeodetic database. The aforementioned spatial gaps represent areas with large uncertainties of 3D elastic dislocation models and are close to hypothetical patch boundaries of the "preferred" model of Wang et al. (2013). Our new estimate is the first step in bringing the density of estimates in this region closer to that of coastal Oregon.

Correlating Variable Subsidence Data for Different Earthquakes among Sites in Southern Cascadia: Significance and Uncertainties

Modern instrumented ruptures suggest that slip during large megathrust earthquakes is heterogenous (e.g., Chlieh et al., 2007; Lee et al., 2011; Lorito et al., 2011; Yokota et al., 2011; Wei et al., 2012), and this is now also suggested by 15 quantitative microfossil-derived coseismic subsidence estimates over ~900 km along the Cascadia margin for the Cascadia subduction zone 1700 CE earthquake (e.g., Wang et al., 2013; Kemp et al., 2018). Heterogenous rupture is also a likely characteristic of earlier earthquakes as well (e.g., Atwater et al., 2005; Shennan et al., 2016; Goldfinger et al., 2012, 2017). Our new results add to data that point to variability in coseismic subsidence estimates by suggesting that the amount of coseismic subsidence has varied between earthquakes. Investigating the spatial variability of coseismic land-level changes over multiple earthquake cycles requires a dense network of quantitative estimates for each earthquake, similar to the current paleogeodetic database of the 1700 CE earthquake.

Extending this record back in time is complicated not only by the sparse current record of precise subsidence estimates (e.g., Milker et al., 2016) but also by the inherent uncertainties in correlating chronologies along the margin reconstructed from radiocarbon age estimates that span centuries or greater. However, by combining recent data sets from Cascadia (e.g., Milker et al., 2016; Nelson et al., 2020) with our results, some initial insights may be gleaned about variability in rupture prior to 1700 CE.

The penultimate earthquake recorded in the land-based paleoseismic record at Cascadia apparently produced less subsidence than the 1700 CE earthquake. Our new record from northern Humboldt Bay demonstrates that the penultimate earthquake at 924–816 cal yr B.P. produced smaller subsidence (0.42 ± 0.37 m) than either the 1700 CE earthquake or two older earthquakes at 1232–1005 cal yr B.P. and 1669–1575 cal yr B.P. (estimates of 0.85 ± 0.46 m, 0.79 ± 0.47 m, and ≥ 0.93 m, respectively). Similarly, at Nehalem River in northern Oregon, subsidence during the 1700 CE and 1568–1361 cal yr B.P. earthquakes was 1.1 ± 0.5 m and 1.0 ± 0.4 m but perhaps as low as 0.7 ± 0.4 m during the penultimate earthquake at 942–764 cal yr B.P. (Nelson et al., 2020), although an estimate from a second site (1.0 ± 0.4 m) suggests a comparable amount of subsidence. The South Slough estuary in southern Oregon shows a similar pattern of variability in subsidence estimates. Evidence from Crown Point (Hawkes et al., 2011) and Talbot Creek (Milker et al., 2016) suggests of subsidence of 0.85 m and 0.36 m, respectively, during the 1700 CE earthquake. Yet, a potential earthquake contact recorded at Talbot Creek with a large age range (1020–545 cal yr B.P.) shows almost no subsidence (0.01 m). This is preceded by an earthquake dated to 1280–1190 cal yr B.P. that produced 0.63–0.65 m of subsidence (Milker et al., 2016). Given the low subsidence estimate for the 1020–545 cal yr B.P. contact, Milker et al. (2016) are rightly cautious in interpreting this as an earthquake as opposed to formation by hydrodynamic processes. However, if this contact was caused by an earthquake that had smaller subsidence amounts, then the Talbot Creek record provides further support for lower subsidence in the land-based record at Cascadia across much of the margin during the penultimate earthquake as compared to during the preceding and following earthquakes.

At northern Humboldt Bay, the penultimate earthquake at ca. 875 cal yr B.P. overlaps with the age distribution of the margin-wide turbidite deposit of T3 (ca. 800 cal yr B.P.), which is inferred to represent a full-margin rupture (Goldfinger et al., 2012). Given the potential evidence for lower subsidence during the ca. 875 cal yr B.P. earthquake, an accompanying margin-wide rupture and tsunami implies that either less slip is required to induce a full-margin turbidite and/or more slip occurred offshore during this earthquake, which suggests that slip distribution varies between great and giant earthquakes at Cascadia. However, because T3 is one of the largest turbidites in the turbidite sequence (Goldfinger et al., 2012), slip distribution seems to be a better explanation for the relatively lower subsidence during the ca. 875 cal yr B.P. earthquake than less slip being required to produce a full-margin rupture. Additional land-based records with high-precision chronologies and microfossil-based estimates of subsidence are required to further evaluate this possibility.

CONCLUSIONS

High-precision chronostratigraphic methods and quantitative RSL reconstructions have refined our understanding of the paleoseismic history at northern Humboldt Bay. The tidal wetland stratigraphy at northern Humboldt Bay contains four stratigraphic sequences (three mud-over-peat contacts and one mud-over-upland soil contact) that are consistent with megathrust-induced subsidence. Based on stratigraphic, chronologic, fossil foraminifera analyses, and timing estimate comparisons to evidence of plate boundary earthquakes at other paleoseismic sites, we conclude that contacts A, C, D, and E record subsidence during past Cascadia subduction zone plate boundary earthquakes. Data for contact B, found only at Mad River Slough, are insufficient to infer that contact B records a great earthquake, and we infer that the contact formed through local nonseismic hydrographic processes associated with the slough. Multiple minimum and maximum limiting ages of in situ plant macrofossils found above and below subsidence contacts, combined with the construction of Bayesian age models, provide the tightest age distributions for three plate boundary earthquakes along the southern Cascadia coastline that are the next oldest after the 1700 CE subduction zone earthquake. These tightly bounded ages are 924–816 cal yr B.P., 1231–1004 cal yr B.P., and 1669–1575 cal yr B.P. (Table 3). The stratigraphic evidence for four plate boundary earthquakes at northern Humboldt Bay corresponds with stratigraphic evidence from six proximal coastal paleoseismic locations (43.5°–40.5°N). In the course of investigating earthquake chronology, we considered sedimentation rate-informed Bayesian age models and decided that within the active plate tectonic setting of coastal wetlands situated on subduction zone margins, an age model using dense sampling around earthquake contacts and no applied sedimentation rate was better than age models that incorporate sedimentation rates.

We reconstruct RSL elevations by applying a foraminiferal Bayesian transfer function to fossil data from representative stratigraphic sequences (three mud-over-peat contacts and one mud-over-upland soil contact) collected at McDaniel Creek marsh and provide the first fully quantitative estimates of coseismic subsidence for northern Humboldt Bay, California. The coseismic subsidence estimates are 0.85 ± 0.46 m for the 1700 CE earthquake, 0.42 ± 0.37 m for the ca. 875 cal yr B.P. earthquake, 0.79 ± 0.47 m for the ca. 1120 cal yr B.P. earthquake, and ≥ 0.93 m for the ca. 1620 cal yr B.P. earthquake (Fig. 5; Table 4). The subsidence estimate for the oldest earthquake is a minimum because the paleoenvironment prior to the earthquake likely formed above the upper limit of foraminiferal habitation (Fig. 5; Table 4). Our coseismic subsidence estimates provide high-resolution data for future modeling of Cascadia earthquakes and offer insight into the inherent variability in coseismic subsidence over multiple earthquake cycles. To further address remaining paleoseismic uncertainties, future Cascadia coastal paleoseismology investigations should seek to address remaining spatial gaps and incorporate high-resolution lithostratigraphic imagery, high-precision dating techniques, and fully quantitative, microfossil-based RSL reconstructions. Specifically, our results highlight the need for additional precise paleoseismic chronologies

and, if possible, coseismic subsidence estimates from southern Cascadia at sites (Fig. 6) such as at Eel River (~40.65°N), southern Humboldt Bay (~40.7°N), Lagoon Creek (~41.9°N), and Sand Mine Marsh (~41.74°N).

ACKNOWLEDGMENTS

This work was supported by the Earthquake Hazards Program of the U.S. Geological Survey (USGS) of the Department of the Interior under USGS award numbers G14AP00128 and G19AP00105 to S.E. Engelhart and G14AP000129 to E. Hemphill-Haley and H.M. Kelsey. The views and conclusions contained in this document are those of the authors and should not be interpreted as necessarily representing the official policies, either express or implied, of the U.S. Government. Research was further supported by the National Science Foundation (EAR-1419844) to S.E. Engelhart and the Northern California Geological Society, Richard Chambers Memorial Scholarship 2017 to J.S. Padgett. We thank Dylan Caldwell for conducting an RTK-GPS survey, Byron Halavik, Erin Quinn, and Casey Loofbourrow for the their field support efforts, Jaime Delano and Alan Nelson for their help with Figure 1A, and the Humboldt State University Geology Department for providing access to field equipment and lab facilities. We thank Science Editor Rob Strachan for overseeing the science review. Reviews by Chris Goldfinger, Lydia Staisch, an anonymous reviewer, and Associate Editor Stefano Mazzoli substantially improved the manuscript. This is a contribution to International Geoscience Program 639—Sea-Level Changes from Minutes to Millennia.

REFERENCES CITED

Abramson, H.F., 1998, Evidence for tsunamis and earthquakes during the last 3500 years from Lagoon Creek, a coastal freshwater marsh, northern California [M.S. thesis]: Arcata, California, Humboldt State University, 62 p.

Adams, J., 1990, Paleoseismicity of the Cascadia subduction zone: Evidence from turbidites off the Oregon-Washington margin: Tectonics, v. 9, no. 4, p. 569–583, https://doi.org/10.1029/TC009i004p00569.

Allen, J.R.L., 1989, Evolution of salt-marsh cliffs in muddy and sandy systems: A qualitative comparison of British west-coast estuaries: Earth Surface Processes and Landforms, v. 14, no. 1, p. 85–92, https://doi.org/10.1002/esp.3290140108.

Allen, J.R.L., 1997, Simulation models of salt-marsh morphodynamics: Some implications for high-intertidal sediment couplets related to sea-level change: Sedimentary Geology, v. 113, no. 3–4, p. 211–223, https://doi.org/10.1016/S0037-0738(97)00101-2.

Allen, J.R., 2000, Morphodynamics of Holocene salt marshes: A review sketch from the Atlantic and Southern North Sea coasts of Europe: Quaternary Science Reviews, v. 19, no. 12, p. 1155–1231, https://doi.org/10.1016/S0277-3791(99)00034-7.

Atwater, B.F., 1987, Evidence for great Holocene earthquakes along the outer coast of Washington State: Science, v. 236, no. 4804, p. 942–944, https://doi.org/10.1126/science.236.4804.942.

Atwater, B.F., 1992, Geologic evidence for earthquakes during the past 2000 years along the Copalis River, southern coastal Washington: Journal of Geophysical Research: Solid Earth, v. 97, no. B2, p. 1901–1919, https://doi.org/10.1029/91JB02346.

Atwater, B.F., and Hemphill-Haley, E., 1997, Recurrence intervals for great earthquakes of the past 3,500 years at northeastern Willapa Bay, Washington: U.S. Geological Survey Professional Paper 1576, 108 p.

Atwater, B.F., and Yamaguchi, D.K., 1991, Sudden, probably coseismic submergence of Holocene trees and grass in coastal Washington State: Geology, v. 19, no. 7, p. 706–709, https://doi.org/10.1130/0091-7613(1991)019<0706:SPCSOH>2.3.CO;2.

Atwater, B.F., Yamaguchi, D.K., Bondevik, S., Barnhardt, W.A., Amidon, L.J., Benson, B.E., Skjerdal, G., Shulene, J.A., and Nanayama, F., 2001, Rapid resetting of an estuarine recorder of the 1964 Alaska earthquake: Geological Society of America Bulletin, v. 113, no. 9, p. 1193–1204, https://doi.org/10.1130/0016-7606(2001)113<1193:RROAER>2.0.CO;2.

Atwater, B.F., Tuttle, M.P., Schweig, E.S., Rubin, C.M., Yamaguchi, D.K., and Hemphill-Haley, E., 2003, Earthquake recurrence inferred from paleoseismology: Developments in Quaternary Sciences, v. 1, p. 331–350, https://doi.org/10.1016/S1571-0866(03)01015-7.

Atwater, B.F., Musumi-Rokkaku, S., Satake, K., Tsuji, Y., Ueda, K., and Yamaguchi, D.K., 2005, The Orphan Tsunami of 1700—Japanese Clues to a Parent Earthquake in North America: U.S. Geological Survey Professional Paper 1707, University of Washington Press, 133 p.

Benson, B.E., Atwater, B.F., Yamaguchi, D.K., Amidon, L.J., Brown, S.L., and Lewis, R.C., 2001, Renewal of tidal forests in Washington State after a subduction earthquake in A.D. 1700: Quaternary Research, v. 56, p. 139–147, https://doi.org/10.1006/qres.2001.2251.

Briggs, R.W., Engelhart, S.E., Nelson, A.R., Dura, T., Kemp, A.C., Haeussler, P.J., Corbett, D.R., Angster, S.J., and Bradley, L.A., 2014, Uplift and subsidence reveal a nonpersistent megathrust rupture boundary (Sitkinak Island, Alaska): Geophysical Research Letters, v. 41, no. 7, p. 2289–2296, https://doi.org/10.1002/2014GL059380.

Bronk Ramsey, C.B., 1995, Radiocarbon calibration and analysis of stratigraphy: The OxCal program: Radiocarbon, v. 37, no. 2, p. 425–430, https://doi.org/10.1017/S0033822200030903.

Bronk Ramsey, C., 2008, Deposition models for chronological records: Quaternary Science Reviews, v. 27, no. 1–2, p. 42–60, https://doi.org/10.1016/j.quascirev.2007.01.019.

Bronk Ramsey, C.B., 2009, Bayesian analysis of radiocarbon dates: Radiocarbon, v. 51, p. 337–360, https://doi.org/10.1017/S0033822200033865.

Bronk Ramsey, C.B., and Lee, S., 2013, Recent and planned developments of the program OxCal: Radiocarbon, v. 55, no. 2, p. 720–730, https://doi.org/10.1017/S0033822200057878.

Cahill, N., Kemp, A.C., Horton, B.P., and Parnell, A.C., 2016, A Bayesian hierarchical model for reconstructing relative sea level: From raw data to rates of change: Climate of the Past, v. 12, no. 2, p. 525–542, https://doi.org/10.5194/cp-12-525-2016.

Cahoon, D.R., Lynch, J.C., and Powell, A.N., 1996, Marsh vertical accretion in a southern California estuary, USA: Estuarine, Coastal and Shelf Science, v. 43, no. 1, p. 19–32, https://doi.org/10.1006/ecss.1996.0055.

Chlieh, M., Avouac, J.P., Hjorleifsdottir, V., Song, T.R.A., Ji, C., Sieh, K., Sladen, A., Hebert, H., Prawirodirdjo, L., Bock, Y., and Galetzka, J., 2007, Coseismic slip and afterslip of the great Mw 9.15 Sumatra–Andaman earthquake of 2004: Bulletin of the Seismological Society of America, v. 97, 1A, p. S152–S173, https://doi.org/10.1785/0120050631.

Clarke, S.H., and Carver, G.A., 1992, Late Holocene tectonics and paleoseismicity, southern Cascadia subduction zone: Science, v. 255, no. 5041, p. 188–192, https://doi.org/10.1126/science.255.5041.188.

Darienzo, M.E., 1987, Late Holocene geologic history of a Netarts Bay salt marsh, northwest Oregon coast, and its relationship to relative sea level changes [M.S. thesis]: Eugene, University of Oregon, Interdisciplinary Studies Program, 94 p.

Darienzo, M.E., and Peterson, C.D., 1990, Episodic tectonic subsidence of late Holocene salt marshes, northern Oregon central Cascadia margin: Tectonics, v. 9, no. 1, p. 1–22, https://doi.org/10.1029/TC009i001p00001.

Darienzo, M.E., Peterson, C.D., and Clough, C., 1994, Stratigraphic evidence for great subduction-zone earthquakes at four estuaries in northern Oregon, USA: Journal of Coastal Research, v. 10, p. 850–876.

Davies, M.H., Mix, A.C., Stoner, J.S., Addison, J.A., Jaeger, J., Finney, B., and Wiest, J., 2011, The deglacial transition on the southeastern Alaska Margin: Meltwater input, sea level rise, marine productivity, and sedimentary anoxia: Paleoceanography and Paleoclimatology, v. 26, no. PA2223, p. 1–18, https://doi.org/10.1029/2010PA002051.

de Rijk, S., 1995, Salinity control on the distribution of salt marsh foraminifera (Great Marshes, Massachusetts): Journal of Foraminiferal Research, v. 25, no. 2, p. 156–166, https://doi.org/10.2113/gsjfr.25.2.156.

Dura, T., Hemphill-Haley, E., Sawai, Y., and Horton, B.P., 2016, The application of diatoms to reconstruct the history of subduction zone earthquakes and tsunamis: Earth-Science Reviews, v. 152, p. 181–197, https://doi.org/10.1016/j.earscirev.2015.11.017.

Dura, T., Horton, B.P., Cisternas, M., Ely, L.L., Hong, I., Nelson, A.R., Wesson, R.L., Pilarczyk, J.E., Parnell, A.C., and Nikitina, D., 2017, Subduction zone slip variability during the last millennium, south-central Chile: Quaternary Science Reviews, v. 175, p. 112–137, https://doi.org/10.1016/j.quascirev.2017.08.023.

Eicher, A.L., 1987, Salt marsh vascular plant distribution in relation to tidal elevation, Humboldt Bay, California [M.S. thesis]: Arcata, California, Humboldt State University, 86 p.

Engelhart, S.E., Horton, B.P., Nelson, A.R., Hawkes, A.D., Witter, R.C., Wang, K., Wang, P.L., and Vane, C.H., 2013a, Testing the use of microfossils to reconstruct great earthquakes at Cascadia: Geology, v. 41, no. 10, p. 1067–1070, https://doi.org/10.1130/G34544.1.

Engelhart, S.E., Horton, B.P., Vane, C.H., Nelson, A.R., Witter, R.C., Brody, S.R., and Hawkes, A.D., 2013b, Modern foraminifera, $\delta^{13}C$, and bulk geochemistry of central Oregon tidal marshes and their application in paleoseismology: Palaeogeography, Palaeoclimatology, Palaeoecology, v. 377, p. 13–27, https://doi.org/10.1016/j.palaeo.2013.02.032.

Engelhart, S.E., Vacchi, M., Horton, B.P., Nelson, A.R., and Kopp, R.E., 2015, A sea-level database for the Pacific coast of central North America: Quaternary Science Reviews, v. 113, p. 78–92, https://doi.org/10.1016/j.quascirev.2014.12.001.

Engelhart, S.E., Hemphill-Haley, E., Kelsey, H.M., and Padgett, J.S., 2016, Refined estimates of coseismic subsidence along the Southern Cascadia Subduction Zone in northern Humboldt Bay (Arcata Bay): U.S. Geological Survey Grant Report, Collaborative Research with University of Rhode Island and Humboldt State University, No. G14AP00128 and G14AP00129, 38 p.

Enkin, R.J., Dallimore, A., Baker, J., Southon, J.R., and Ivanochko, T., 2013, A new high-resolution radiocarbon Bayesian age model of the Holocene and Late Pleistocene from core MD02–2494 and others, Effingham Inlet, British Columbia, Canada; with an application to the paleoseismic event chronology of the Cascadia Subduction Zone: Canadian Journal of Earth Sciences, v. 50, no. 7, p. 746–760, https://doi.org/10.1139/cjes-2012-0150.

Fatela, F., and Taborda, R., 2002, Confidence limits of species proportions in microfossil assemblages: Marine Micropaleontology, v. 45, no. 2, p. 169–174, https://doi.org/10.1016/S0377-8398(02)00021-X.

Friedrichs, C.T., and Perry, J.E., 2001, Tidal salt marsh morphodynamics: A synthesis: Journal of Coastal Research, v. 27, p. 7–37.

Gabet, E.J., 1998, Lateral migration and bank erosion in a saltmarsh tidal channel in San Francisco Bay, California: Estuaries, v. 21, no. 4, p. 745–753, https://doi.org/10.2307/1353278.

Garrett, E., Shennan, I., Woodroffe, S.A., Cisternas, M., Hocking, E.P., and Gulliver, P., 2015, Reconstructing paleoseismic deformation, 2: 1000 years of great earthquakes at Chucalén, south central Chile: Quaternary Science Reviews, v. 113, p. 112–122, https://doi.org/10.1016/j.quascirev.2014.10.010.

Garrison-Laney, C.E., 1998, Diatom evidence for tsunami inundation from Lagoon Creek, a coastal freshwater pond, Del Norte County, California [M.S. thesis]: Arcata, California, Humboldt State University, 97 p.

GEBCO Bathymetric Compilation Group, 2019, The GEBCO_2019 Grid—a continuous terrain model of the global oceans and land: British Oceanographic data Centre, National Oceanography Centre, NERC, UK, https://www.doi.org/10/c33m.

Goldfinger, C., Nelson, C.H., Morey, A.E., Johnson, J.E., Patton, J.R., Karabanov, E.B., Gutierrez-Pastor, J.,

Eriksson, A.T., Gracia, E., Dunhill, G., and Enkin, R.J., 2012, Turbidite event history—Methods and implications for Holocene paleoseismicity of the Cascadia subduction zone: U.S. Geological Survey Professional Paper 1661-F, 170 p.

Goldfinger, C., Morey, A.E., Black, B., Beeson, J., Nelson, C.H., and Patton, J., 2013, Spatially limited mud turbidites on the Cascadia margin: Segmented earthquake ruptures?: Natural Hazards and Earth System Sciences, v. 13, no. 8, p. 2109, https://doi.org/10.5194/nhess-13-2109-2013.

Goldfinger, C., Galer, S., Beeson, J., Hamilton, T., Black, B., Romsos, C., Patton, J., Nelson, C.H., Hausmann, R., and Morey, A., 2017, The importance of site selection, sediment supply, and hydrodynamics: A case study of submarine paleoseismology on the northern Cascadia margin, Washington USA: Marine Geology, v. 384, p. 4–46, https://doi.org/10.1016/j.margeo.2016.06.008.

Graehl, N.A., Kelsey, H.M., Witter, R.C., Hemphill-Haley, E., and Engelhart, S.E., 2015, Stratigraphic and microfossil evidence for a 4500-year history of Cascadia subduction zone earthquakes and tsunamis at Yaquina River estuary, Oregon, USA: Geological Society of America Bulletin, v. 127, no. 1–2, p. 211–226, https://doi.org/10.1130/B31074.1.

Guilbault, J.P., Clague, J.J., and Lapointe, M., 1995, Amount of subsidence during a late Holocene earthquake—Evidence from fossil tidal marsh foraminifera at Vancouver Island, west coast of Canada: Palaeogeography, Palaeoclimatology, Palaeoecology, v. 118, no. 1, p. 49–71, https://doi.org/10.1016/0031-0182(94)00135-U.

Guilbault, J.P., Clague, J.J., and Lapointe, M., 1996, Foraminiferal evidence for the amount of coseismic subsidence during a late Holocene earthquake on Vancouver Island, west coast of Canada: Quaternary Science Reviews, v. 15, no. 8, p. 913–937, https://doi.org/10.1016/S0277-3791(96)00058-3.

Haslett, J., and Parnell, A., 2008, A simple monotone process with application to radiocarbon-dated depth chronologies: Journal of the Royal Statistical Society. Series C: Applied Statistics, v. 57, no. 4, p. 399–418, https://doi.org/10.1111/j.1467-9876.2008.00623.x.

Hawkes, A.D., Horton, B.P., Nelson, A.R., and Hill, D.F., 2010, The application of intertidal foraminifera to reconstruct coastal subsidence during the giant Cascadia earthquake of AD 1700 in Oregon, USA: Quaternary International, v. 221, no. 1, p. 116–140, https://doi.org/10.1016/j.quaint.2009.09.019.

Hawkes, A.D., Horton, B.P., Nelson, A.R., Vane, C.H., and Sawai, Y., 2011, Coastal subsidence in Oregon, USA, during the giant Cascadia earthquake of AD 1700: Quaternary Science Reviews, v. 30, no. 3, p. 364–376, https://doi.org/10.1016/j.quascirev.2010.11.017.

Hemphill-Haley, E., 1995, Diatom evidence for earthquake-induced subsidence and tsunami 300 yr ago in southern coastal Washington: Geological Society of America Bulletin, v. 107, no. 3, p. 367–378, https://doi.org/10.1130/0016-7606(1995)107<0367:DEFEIS>2.3.CO;2.

Hemphill-Haley, E., Kelsey, H.M., Graehl, N., Casso, M., Caldwell, D., Loofbourrow, C., Robinson, M., Vermeer, J., and Southwick, E., 2019, Recent sandy deposits at five northern California coastal wetlands—Stratigraphy, diatoms, and implications for storm and tsunami hazards: U.S. Geological Survey Scientific Investigations Report 2018–5111, 187 p., https://doi.org/10.3133/sir20185111.

Holden, P.B., Birks, H.J.B., Brooks, S.J., Bush, M.B., Hwang, G.M., Matthews-Bird, F., Valencia, B.G., and Van Woesik, R., 2017, BUMPER v 1. 0: A Bayesian user-friendly model for palaeo-environmental reconstruction.

Horton, B.P., and Edwards, R.J., 2005, The application of local and regional transfer functions to the reconstruction of Holocene sea levels, north Norfolk, England: The Holocene, v. 15, no. 2, p. 216–228, https://doi.org/10.1191/0959683605hl787rp.

Horton, B.P., and Edwards, R.J., 2006, Quantifying Holocene Sea Level Change Using Intertidal Foraminifera: Lessons from the British Isles: Cushman Foundation for Foraminiferal Research Special Publication, v. 40, 97 p.

Jennings, A.E., and Nelson, A.R., 1992, Foraminiferal assemblage zones in central Oregon salt marshes—Relation to marsh floristic zones and sea level: Journal of Foraminiferal Research, v. 22, no. 1, p. 13–29, https://doi.org/10.2113/gsjfr.22.1.13.

Kelsey, H.M., Witter, R.C., and Hemphill-Haley, E., 2002, Plate-boundary earthquakes and tsunamis of the past 5500 yr, Sixes River estuary, southern Oregon: Geological Society of America Bulletin, v. 114, no. 3, p. 298–314, https://doi.org/10.1130/0016-7606(2002)114<0298:PBEATO>2.0.CO;2.

Kelsey, H.M., Nelson, A.R., Witter, R.C., and Hemphill-Haley, E., 2005, Tsunami history of an Oregon coastal lake reveals a 4,600 year record of great earthquakes on the Cascadia subduction zone: Geological Society of America Bulletin, v. 117, p. 1009–1032, https://doi.org/10.1130/B25452.1.

Kelsey, H.M., Engelhart, S.E., Pilarczyk, J.E., Horton, B.P., Rubin, C.M., Daryono, M.R., Ismail, N., Hawkes, A.D., Bernhardt, C.E., and Cahill, N., 2015, Accommodation space, relative sea level, and the archiving of paleoearthquakes along subduction zones: Geology, v. 43, no. 8, p. 675–678, https://doi.org/10.1130/G36706.1.

Kemp, A.C., and Telford, R.J., 2015, Transfer functions, *in* Shennan, I., Long, A.J., and Horton, B.P., eds., Handbook of sea-level research: John Wiley & Sons, American Geophysical Union, p. 470–499.

Kemp, A.C., Horton, B.P., Culver, S.J., Corbett, D.R., van de Plassche, O., Gehrels, W.R., Douglas, B.C., and Parnell, A.C., 2009, Timing and magnitude of recent accelerated sea-level rise (North Carolina, United States): Geology, v. 37, no. 11, p. 1035–1038, https://doi.org/10.1130/G30352A.1.

Kemp, A.C., Horton, B.P., Donnelly, J.P., Mann, M.E., Vermeer, M., and Rahmstorf, S., 2011, Climate related sea-level variations over the past two millennia: Proceedings of the National Academy of Sciences of the United States of America, v. 108, no. 27, p. 11017–11022, https://doi.org/10.1073/pnas.1015619108.

Kemp, A.C., Nelson, A.R., and Horton, B.P., 2013, Radiocarbon dating of plant macrofossils from tidal-marsh sediment, *in* Shroder, J.F., ed., Treatise on Geomorphology, v. 14: San Diego, Academic Press, p. 370–388, https://doi.org/10.1016/B978-0-12-374739-6.00400-0.

Kemp, A.C., Cahill, N., Engelhart, S.E., Hawkes, A.D., and Wang, K., 2018, Revising estimates of spatially variable subsidence during the AD 1700 Cascadia earthquake using a Bayesian foraminiferal transfer function: Bulletin of the Seismological Society of America, v. 108, no. 2, p. 654–673, https://doi.org/10.1785/0120170269.

Lee, S.J., Huang, B.S., Ando, M., Chiu, H.C., and Wang, J.H., 2011, Evidence of large scale repeating slip during the 2011 Tohoku-Oki earthquake: Geophysical Research Letters, v. 38, no. 19, https://doi.org/10.1029/2011GL049580.

Letzsch, W.S., and Frey, R.W., 1980, Deposition and erosion in a Holocene salt marsh, Sapelo Island, Georgia: Journal of Sedimentary Research, v. 50, no. 2, p. 529–542.

Li, W.H., 1992, Evidence for the late Holocene coseismic subsidence in the Lower Eel River valley, Humboldt County, Northern California: An application of foraminiferal zonation to indicate tectonic submergence [M.S. thesis]: Arcata, California, Humboldt State University, 93 p.

Long, A.J., and Shennan, I., 1994, Sea-level changes in Washington and Oregon and the" earthquake deformation cycle: Journal of Coastal Research, v. 10, no. 4, p. 825–838.

Lorito, S., Romano, F., Atzori, S., Tong, X., Avallone, A., McCloskey, J., Cocco, M., Boschi, E., and Piatanesi, A., 2011, Limited overlap between the seismic gap and coseismic slip of the great 2010 Chile earthquake: Nature Geoscience, v. 4, no. 3, p. 173, https://doi.org/10.1038/ngeo1073.

Mariotti, G., Kearney, W.S., and Fagherazzi, S., 2016, Soil creep in salt marshes: Geology, v. 44, no. 6, p. 459–462, https://doi.org/10.1130/G37708.1.

Milker, Y., Horton, B.P., Vane, C.H., Engelhart, S.E., Nelson, A.R., Witter, R.C., Khan, N.S., and Bridgeland, W.T., 2015, Annual and seasonal distribution of intertidal foraminifera and stable carbon isotope geochemistry, Bandon Marsh, Oregon, USA: Journal of Foraminiferal Research, v. 45, no. 2, p. 146–155, https://doi.org/10.2113/gsjfr.45.2.146.

Milker, Y., Nelson, A.R., Horton, B.P., Engelhart, S.E., Bradley, L.-A., and Witter, R.C., 2016, Differences in coastal subsidence in southern Oregon (USA) during at least six prehistoric megathrust earthquakes: Quaternary Science Reviews, v. 142, p. 143–163, https://doi.org/10.1016/j.quascirev.2016.04.017.

Nelson, A.R., 1992, Discordant ^{14}C ages from buried tidal-marsh soils in the Cascadia subduction zone, southern Oregon coast: Quaternary Research, v. 38, no. 1, p. 74–90, https://doi.org/10.1016/0033-5894(92)90031-D.

Nelson, A.R., 2015, Coastal sediments, *in* Shennan, I., Long, A.J., and Horton, B.P., eds., Handbook of Sea-Level Research: John Wiley & Sons, American Geophysical Union, p.47–65.

Nelson, A.R., Atwater, B.F., Bobrowsky, P.T., Bradley, L.A., Clague, J.J., Carver, G.A., Darienzo, M.E., Grant, W.C., Krueger, H.W., Sparks, R., and Stafford, T.W., 1995, Radiocarbon evidence for extensive plate-boundary rupture about 300 years ago at the Cascadia subduction zone: Nature, v. 378, no. 6555, p. 371–374, https://doi.org/10.1038/378371a0.

Nelson, A.R., Shennan, I., and Long, A.J., 1996a, Identifying coseismic subsidence in tidal-wetland stratigraphic sequences at the Cascadia subduction zone of western North America: Journal of Geophysical Research: Solid Earth, v. 101, no. B3, p. 6115–6135, https://doi.org/10.1029/95JB01051.

Nelson, A.R., Jennings, A.E., and Kashima, K., 1996b, An earthquake history derived from stratigraphic and microfossil evidence of relative sea-level change at Coos Bay, southern coastal Oregon: Geological Society of America Bulletin, v. 108, no. 2, p. 141–154, https://doi.org/10.1130/0016-7606(1996)108<0141:AEHDFS>2.3.CO;2.

Nelson, A.R., Ota, Y., Umitsu, M., Kashima, K., and Matsushima, Y., 1998, Seismic or hydrodynamic control of rapid late-Holocene sea-level rises in southern coastal Oregon, USA?: The Holocene, v. 8, no. 3, p. 287–299, https://doi.org/10.1191/095968398668600476.

Nelson, A.R., Asquith, A.C., and Grant, W.C., 2004, Great earthquakes and tsunamis of the past 2000 years at the Salmon River estuary, central Oregon coast, USA: Bulletin of the Seismological Society of America, v. 94, no. 4, p. 1276–1292, https://doi.org/10.1785/012003210.

Nelson, A.R., Kelsey, H.M., and Witter, R.C., 2006, Great earthquakes of variable magnitude at the Cascadia subduction zone: Quaternary Research, v. 65, p. 354–365, https://doi.org/10.1016/j.yqres.2006.02.009.

Nelson, A.R., Sawai, Y., Jennings, A.E., Bradley, L.A., Gerson, L., Sherrod, B.L., Sabean, J., and Horton, B.P., 2008, Great-earthquake paleogeodesy and tsunamis of the past 2000 years at Alsea Bay, central Oregon coast, USA: Quaternary Science Reviews, v. 27, no. 7, p. 747–768, https://doi.org/10.1016/j.quascirev.2008.01.001.

Nelson, A.R., Hawkes, A.D., Sawai, Y., Engelhart, S.E., Witter, R., Grant-Walter, W.C., Bradley, L.A., Dura, T., Cahill, N., and Horton, B., 2020, Identifying the greatest earthquakes of the past 2000 years at the Nehalem River Estuary, Northern Oregon Coast, USA: OpenQuaternary, v. 6, no. 2, p. 1–30, https://doi.org/10.5334/oq.70.

Parnell, A.C., Haslett, J., Allen, J.R., Buck, C.E., and Huntley, B., 2008, A flexible approach to assessing synchroneity of past events using Bayesian reconstructions of sedimentation history: Quaternary Science Reviews, v. 27, no. 19–20, p. 1872–1885, https://doi.org/10.1016/j.quascirev.2008.07.009.

Patton, J., 2004, Late Holocene coseismic subsidence and coincident tsunamis, southern Cascadia subduction zone, Hookton Slough, Humboldt Bay, California [M.S. thesis]: Arcata, California, Humboldt State University, 76 p.

Peterson, C.D., and Darienzo, M.E., 1991, Discrimination of climatic, oceanic and tectonic forcing of marsh burial events from Alsea Bay, Oregon, USA, *in* Rogers, A.M., Walsh, T.J., Kockelman, W.J., and Priest, G.R., eds., Assessing and reducing earthquake hazards in the Pacific Northwest: U.S. Geological Survey Open-File Report 91-441C, p. 1–53.

Peterson, C.D., Carver, G.A., Cruikshank, K.M., Abramson, H.F., Garrison-Laney, C.E., and Dengler, L.A., 2011, Evaluation of the use of paleotsunami deposits to reconstruct inundation distance and runup heights associated with prehistoric inundation events, Crescent City, southern Cascadia margin: Earth Surface Processes and Landforms, v. 36, no. 7, p. 967–980, https://doi.org/10.1002/esp.2126.

Pickart, A.J., and Hesp, P.A., 2019, Spatio-temporal geomorphological and ecological evolution of a transgressive dunefield system, Northern California, USA: Global and Planetary Change, v. 172, p. 88–103, https://doi.org/10.1016/j.gloplacha.2018.09.012.

Pilarczyk, J.E., Dura, T., Horton, B.P., Engelhart, S.E., Kemp, A.C., and Sawai, Y., 2014, Microfossils from coastal environments as indicators of paleo-earthquakes, tsunamis and storms: Palaeogeography, Palaeoclimatology, Palaeoecology, v. 413, p. 144–157, https://doi.org/10.1016/j.palaeo.2014.06.033.

Pritchard, C.J., 2004, Late Holocene relative sea-level changes, Arcata Bay, California: Evaluation of freshwater syncline movement using coseismically buried soil horizons [M.S. thesis]: Arcata, California, Humboldt State University.

Reimer, P.J., Bard, E., Bayliss, A., Beck, J.W., Blackwell, P.G., Ramsey, C.B., Buck, C.E., Cheng, H., Edwards, R.L., Friedrich, M., and Grootes, P.M., 2013, IntCal13 and Marine13 radiocarbon age calibration curves 0–50,000 years cal BP: Radiocarbon, v. 55, no. 4, p. 1869–1887, https://doi.org/10.2458/azu_js_rc.55.16947.

Rothwell, R.G., and Rack, F.R., 2006, New techniques in sediment core analysis: An introduction, *in* Rothwell, R.G., eds., New Techniques in Sediment Core Analysis: Geological Society, London, Special Publication 267, no. 1, p. 1–29, https://doi.org/10.1144/GSL.SP.2006.267.01.01.

Satake, K., Shimazaki, K., Tsuji, Y., and Ueda, K., 1996, Time and size of a giant earthquake in Cascadia inferred from Japanese tsunami records of January 1700: Nature, v. 379, no. 6562, p. 246–249, https://doi.org/10.1038/379246a0.

Satake, K., Wang, K., and Atwater, B.F., 2003, Fault slip and seismic moment of the 1700 Cascadia earthquake inferred from Japanese tsunami descriptions: Journal of Geophysical Research: Solid Earth, v. 108, B11.

Schlosser, S., and Eicher, A., 2012, The Humboldt Bay and Eel River Estuary Benthic Habitat Project: California Sea Grant Publication T-075, 246 p.

Scott, D.B., and Medioli, F.S., 1982, Micropaleontological documentation for early Holocene fall of relative sea level on the Atlantic coast of Nova Scotia: Geology, v. 10, no. 5, p. 278–281, https://doi.org/10.1130/0091-7613(1982)10<278:MDFEHF>2.0.CO;2.

Shennan, I., Long, A.J., Rutherford, M.M., Green, F.M., Innes, J.B., Lloyd, J.M., Zong, Y., and Walker, K.J., 1996, Tidal marsh stratigraphy, sea-level change and large earthquakes, I: A 5000 year record in Washington, USA: Quaternary Science Reviews, v. 15, no. 10, p. 1023–1059, https://doi.org/10.1016/S0277-3791(96)00007-8.

Shennan, I., Garrett, E., and Barlow, N., 2016, Detection limits of tidal-wetland sequences to identify variable rupture modes of megathrust earthquakes: Quaternary Science Reviews, v. 150, p. 1–30, https://doi.org/10.1016/j.quascirev.2016.08.003.

Simms, A.R., DeWitt, R., Zurbuchen, J., and Vaughan, P., 2017, Coastal erosion and recovery from a Cascadia subduction zone earthquake and tsunami: Marine Geology, v. 392, p. 30–40, https://doi.org/10.1016/j.margeo.2017.08.009.

Törnqvist, T.E., Rosenheim, B.E., Hu, P., and Fernandez, A.B., 2015, Radiocarbon dating and calibration, *in* Shennan, I., Long, A.J., and Horton, B.P., eds., Handbook of Sea-Level Research: John Wiley & Sons, American Geophysical Union, p. 349–360.

Trachsel, M., and Telford, R.J., 2017, All age–depth models are wrong, but are getting better: The Holocene, v. 27, no. 6, p. 860–869, https://doi.org/10.1177/0959683616675939.

Troels-Smith, J., 1955, Karakterisering af lose jordarter (Characterization of unconsolidated sediments): Danmarks Geologiske Undersogelse, v. 3, p. 39-73.

Valentine, D.W., 1992, Late Holocene stratigraphy, Humboldt Bay, California: Evidence for late Holocene paleoseismicity of the southern Cascadia subduction zone [M.S. thesis]: Arcata, California, Humboldt State University, 84 p.

Valentine, D.W., Keller, E.A., Carver, G., Li, W.H., Manhart, C., and Simms, A.R., 2012, Paleoseismicity of the southern end of the Cascadia subduction zone, northwestern California: Bulletin of the Seismological Society of America, v. 102, no. 3, p. 1059–1078, https://doi.org/10.1785/0120110103.

Vick, G.S., 1988, Late Holocene paleoseismicity and relative sea level changes of the Mad River Slough, northern Humboldt Bay, California [M.S. thesis]: Arcata, California, Humboldt State University, 87 p.

Wang, P.L., Engelhart, S.E., Wang, K., Hawkes, A.D., Horton, B.P., Nelson, A.R., and Witter, R.C., 2013, Heterogeneous rupture in the great Cascadia earthquake of 1700 inferred from coastal subsidence estimates: Journal of Geophysical Research: Solid Earth, v. 118, no. 5, p. 2460–2473, https://doi.org/10.1002/jgrb.50101.

Wei, S., Graves, R., Helmberger, D., Avouac, J.P., and Jiang, J., 2012, Sources of shaking and flooding during the Tohoku-Oki earthquake: A mixture of rupture styles: Earth and Planetary Science Letters, v. 333, p. 91–100, https://doi.org/10.1016/j.epsl.2012.04.006.

Witter, R.C., Kelsey, H.M., and Hemphill-Haley, E., 2001, Pacific storms, El Niño and tsunamis: Competing mechanisms for sand deposition in a coastal marsh, Euchre Creek, Oregon: Journal of Coastal Research, v. 17, p. 563–583.

Witter, R.C., Kelsey, H.M., and Hemphill-Haley, E., 2003, Great Cascadia earthquakes and tsunamis of the past 6700 years, Coquille River estuary, southern coastal Oregon: Geological Society of America Bulletin, v. 115, no. 10, p. 1289–1306, https://doi.org/10.1130/B25189.1.

Witter, R., Briggs, R., Engelhart, S.E., Gelfenbaum, G., Koehler, R.D., Nelson, A., Selle, S.L., Corbett, R., and Wallace, K., 2019, Evidence for frequent, large tsunamis spanning locked and creeping parts of the Aleutian megathrust: Geological Society of America Bulletin, v. 131, no. 5–6, p. 707–729, https://doi.org/10.1130/B32031.1.

Wright, A.J., Edwards, R.J., van de Plassche, O., Blaauw, M., Parnell, A.C., van der Borg, K., de Jong, A.F., Roe, H.M., Selby, K., and Black, S., 2017, Reconstructing the accumulation history of a saltmarsh sediment core: Which age-depth model is best?: Quaternary Geochronology, v. 39, p. 35–67, https://doi.org/10.1016/j.quageo.2017.02.004.

Yokota, Y., Koketsu, K., Fujii, Y., Satake, K., Sakai, S.I., Shinohara, M., and Kanazawa, T., 2011, Joint inversion of strong motion, teleseismic, geodetic, and tsunami datasets for the rupture process of the 2011 Tohoku earthquake: Geophysical Research Letters, v. 38, no. 7, https://doi.org/10.1029/2011GL050098.

Science Editor: Rob Strachan
Associate Editor: Stefano Mazzoli

Manuscript Received 25 March 2020
Revised Manuscript Received 24 September 2020
Manuscript Accepted 19 November 2020

Printed in the USA